A TRIDENT SCHOLAR PROJECT REPORT

NO. 511

Wireless Electromechanical Power Transfer Using Piezoelectric Materials

by

Midshipman 1/C Natalie A. Schieuer, USN

UNITED STATES NAVAL ACADEMY
ANNAPOLIS, MARYLAND

USNA-1531-2

REPORT DOCUMENTATION PAGE

Form Approved
OMB No. 0704-0188

1. REPORT DATE *(DD-MM-YYYY)* 7/12/21	**2. REPORT TYPE**	**3. DATES COVERED** *(From - To)*

4. TITLE AND SUBTITLE
Wireless Electromechanical Power Transfer Using Piezoelectric Materials

5a. CONTRACT NUMBER

5b. GRANT NUMBER

5c. PROGRAM ELEMENT NUMBER

6. AUTHOR(S)
Schieuer, Natalie A.

5d. PROJECT NUMBER

5e. TASK NUMBER

5f. WORK UNIT NUMBER

7. PERFORMING ORGANIZATION NAME(S) AND ADDRESS(ES)

8. PERFORMING ORGANIZATION REPORT NUMBER

9. SPONSORING / MONITORING AGENCY NAME(S) AND ADDRESS(ES)
U.S. Naval Academy
Annapolis, MD 21402

10. SPONSOR/MONITOR'S ACRONYM(S)

11. SPONSOR/MONITOR'S REPORT NUMBER(S)
Trident Scholar Report no. 511 (2021)

12. DISTRIBUTION / AVAILABILITY STATEMENT

This document has been approved for public release; its distribution is UNLIMITED.

13. SUPPLEMENTARY NOTES

14. ABSTRACT
In military applications, as well as civilian applications, the use of piezoelectric materials instead of wires allows for reduced mass in power transfer, which is especially applicable to systems designed for flight and/or for orbit. This research has focused on optimizing the location and size of a system of piezoelectric actuators used to transfer electrical power via transduction from electrical voltage to mechanical vibrations and back to electrical voltage. The research project developed models of the system of interest using COMSOL Multiphysics to consider solid mechanics, viscoelasticity, piezoelectricity, electrostatics, electrical circuits and by introducing structural acoustic coupling. The accuracy of the computational model was validated by comparison with published experimental results for existing hardware. The COMSOL model was used in a computational parametric study of electrical transfer efficiency versus the mechanical and geometric parameters for a single piezoelectric transmitter/receiver pair, where the electrical transfer efficiency is defined as the ratio of the power output to the power input. Through the results of this parametric study, guidelines as to what configurations are responsive and unresponsive for a given excitation frequency were developed. These results led to the novel investigation of the single transmitter/multiple receiver array used to selectively excite a target receiver with a single transmitter.

15. SUBJECT TERMS
Piezoelectric, wireless, power efficiency

16. SECURITY CLASSIFICATION OF:			**17. LIMITATION OF ABSTRACT**	**18. NUMBER OF PAGES**	**19a. NAME OF RESPONSIBLE PERSON**
a. REPORT	**b. ABSTRACT**	**c. THIS PAGE**		52	**19b. TELEPHONE NUMBER** *(include area code)*

U.S.N.A. --- Trident Scholar project report; no. 511 (2021)

WIRELESS ELECTROMECHANICAL POWER TRANSFER USING PIEZOELECTRIC MATERIALS

by

Midshipman 1/C Natalie A. Schieuer
United States Naval Academy
Annapolis, Maryland

Certification of Advisers Approval

Associate Professor Joshua J. Radice
Mechanical Engineering Department

Associate Professor John Burkhardt
Mechanical Engineering Department

Acceptance for the Trident Scholar Committee

Professor Maria J. Schroeder
Associate Director of Midshipman Research

USNA-1531-2

Abstract:

With the realities of a finite defense budget, efficient systems for power transfer are vitally important for a wide array of applications such as surface ships, submarines, and weapons systems. Piezoelectric materials are an excellent choice for electromechanical power transfer applications owing to their bidirectional conversion between electrical signal and mechanical response. Piezoelectric materials are a specific type of smart materials that are characterized by their ability to induce an electrical charge when subject to a mechanical strain. This phenomenon is bidirectional as it can be observed in reverse, as piezoelectric materials will also undergo mechanical strain when an electrical voltage is induced (Ramadan et al., 2014). In military applications, as well as civilian applications, the use of piezoelectric materials instead of wires allows for reduced mass in power transfer, which is especially applicable to systems designed for flight and/or for orbit. This research has focused on optimizing the location and size of a system of piezoelectric actuators used to transfer electrical power via transduction from electrical voltage to mechanical vibrations and back to electrical voltage.

The research project developed models of the system of interest using COMSOL Multiphysics to consider solid mechanics, viscoelasticity, piezoelectricity, electrostatics, electrical circuits and by introducing structural acoustic coupling. The accuracy of the computational model was validated by comparison with published experimental results for existing hardware. The COMSOL model was used in a computational parametric study of electrical transfer efficiency versus the mechanical and geometric parameters for a single piezoelectric transmitter/receiver pair, where the electrical transfer efficiency is defined as the ratio of the power output to the power input. Through the results of this parametric study, guidelines as to what configurations are responsive and unresponsive for a given excitation frequency were developed. These results led to the novel investigation of the single transmitter/multiple receiver array used to selectively excite a target receiver with a single transmitter.

Keywords: piezoelectric, wireless, power efficiency

Acknowledgements

Thank you to Dr. Joshua Radice and Dr. John Burkhardt for their willingness to advise me throughout this process and for all of their time they have volunteered. I am so thankful for their guidance they have provided over many Google Meet calls in the Summer, Fall, Spring and in the lab. Thank you to Dr. Sarah Bedair and Dr. Victor Tseng from the Army Research Laboratory for all the assistance and insight they have provided. Thank you to CAPT Brad Baker for graciously allowing me to access the laboratory facilities to conduct my experimental work. Thank you to Mr. Gary Gibson for all of the assistance he has provided in the laboratory. Thank you to Dr. Daniel Opila and Dr. Gregory Sinsley for their insight on the Electrical Engineering aspects of my project and their willingness to meet with me and provide laboratory space in Hopper Hall for additional power measurements. Finally, thank you to Dr. Maria Schroeder and all of the members of the Trident Committee who make the Trident Scholar program possible.

Table of Contents:

Contents

Introduction

With the increasing demand for energy and mass efficient systems in the civilian and military sectors, piezoelectric materials offer a promising and exciting means of electromechanical energy conversion. For example, ambient mechanical energy harvesting is a common and widely researched application of piezoelectric materials. In this application, ambient vibrational energy from environmental sources can be transformed into useful electrical energy via the utilization of the unique properties of piezoelectric materials whereby mechanical deformation results in the development of electrical charge across the piezoelectric domain (Mehraeen et al., 2010). This research specifically explored the application of piezoelectric materials to wireless power transfer as an alternative to power transfer using wires. This use of piezoelectric materials applies to systems that seek to minimize the overall system's mass, such as applications for flight and/or for orbit. This research studied the optimization of the location and size of a system of piezoelectric actuators used for wireless power transfer by first developing computational models of the system of interest using COMSOL Multiphysics for a single transmitter/single receiver case. Considerations for solid mechanics, viscoelasticity, piezoelectricity, electrostatics, electrical circuits and the introduction of structural acoustic coupling were made. The developed model was further refined after comparison to published experimental and computational results. A series of computational parametric studies were conducted and the conclusions reached through these studies assisted in the study of a single transmitter/multiple receiver case by which a user could selectively excite a target receiver with a single transmitter. This report begins with a background of piezoelectric materials, followed by a literature study of past and current research of the applications of these so-called smart materials. Then the report discusses the methodology for the Trident research and discusses the results of the various phases of the project, including the model development, the computational parametric studies, the experimental testing, and the single transmitter/multiple receiver system study.

Background

The Curie brothers are credited with first observing the piezoelectric effect in 1880. The direct piezoelectric effect describes how certain materials will induce an electrical field while undergoing mechanical strain. The indirect piezoelectric effect is the reverse of this process in that an induced electrical field will result in mechanical strain within piezoelectric materials (Ramadan et al., 2014). This makes piezoelectric materials uniquely suited to act as transducers, as they can both act as sensors through the direct piezoelectric effect, and as actuators through the indirect piezoelectric effect (Vijaya, 2013). 'Piezo' comes from the Greek word for pressure, referring to the mechanical pressure or stress that generates electrical polarization in piezoelectric materials (Jalili, 2010). The piezoelectric effect can be observed in several different materials, including polymers (Ramadan et al., 2014) and ceramics (Randeraat, 1968). Different forms of piezoelectric polymers are outlined in Figure 1.

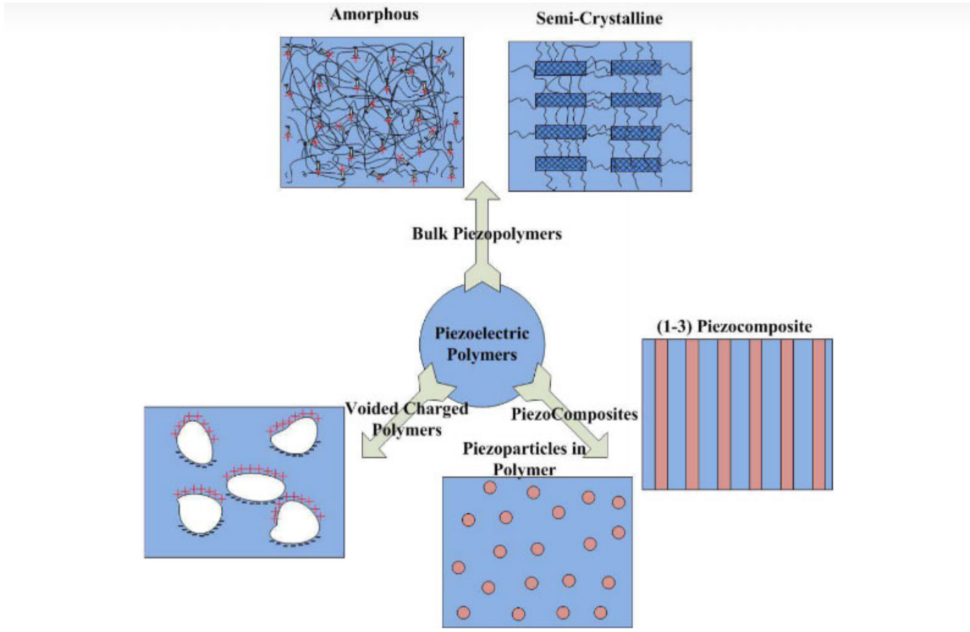

Figure 1: Illustrated Outline of Different Piezoelectric Polymer types (Ramadan et al., 2014)

The piezoelectric effect can be observed in natural materials such as quartz, Rochelle salt (Randeraat, 1968), and even bone (Lee et al., 2012). Researchers have even explored genetically engineering M13 bacteriophage as an alternative to other piezoelectric materials that may involve toxic fabrication methods (Lee et al., 2012).

Lead Zirconate Titanate, known as PZT, is a ubiquitous example of a piezoelectric ceramic (Vijaya, 2013) that is used in everyday devices (Howells, 2009). PZT has high piezoelectric coefficients which are beneficial in obtaining large power outputs (Jung et al., 2011). As is the case with other piezoelectric materials, when a PZT crystal experiences mechanical strain, the dipoles within the crystal align creating a net electric potential across the crystal (Howells, 2009). This alignment of dipoles is illustrated in Figure 2.

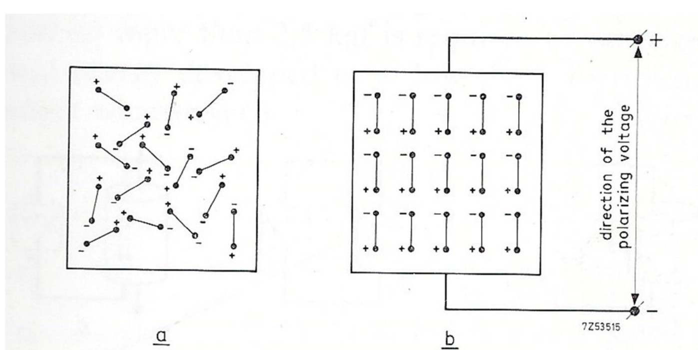

Figure 2: Illustration of Alignment of Dipoles in Polarization Process of Piezoelectric Ceramics (Randeraat, 1968)

Advances in the implementation of piezoelectric materials will not only benefit the Navy and the Department of Defense, but there are also many useful civilian applications in a variety of disciplines. A familiar example is the use of PZT in gas lighters: when stress is applied, the voltage that results eventually causes the spark needed for the lighter through dielectric breakdown (Vijaya, 2013).

A considerable amount of recent research has been working towards the use of piezoelectric materials in energy harvesting applications to supplement or even replace conventional batteries as power sources in specific applications (Mehraeen et al., 2010). In this context, piezoelectric materials can serve as an alternative to batteries as they can be used to convert ambient vibrational energy from the environment into useful electrical energy and stored until needed. In this application, piezoelectric materials are used as energy harvesters that collect vibrational energy from the environment that is often wasted and unused. They can be useful as an alternative to batteries in powering location sensors in wild animals (Chen et al., 2014) or in monitoring sensors that ensure structural health in buildings or bridges (Mehraeen et al., 2010) or any number of other remote location applications. Other research is exploring replacing batteries for pacemakers by capturing mechanical energy from the natural vibrations of the heart or lungs and then converting this into useful electrical energy. This alternative for batteries is advantageous for pacemaker patients as batteries must be surgically replaced, which exposes patients to risk of infection and other complications (Dagdeviren et al., 2014). Other studies have investigated converting energy from human steps into electrical energy to power electronic devices such as GPS, sensors, cell phones, or pagers (Howells, 2009). Piezoelectric materials have also been used for structural vibration control applications (J.-C. Lin & Nien, 2005). Many researchers have devoted time in studying their application to smart structures, which adapt to changing environmental conditions to maintain structural integrity (Liu et al., 1999).

System of Interest:

The Army Research Laboratory (ARL) has expressed a specific interest in the use of piezoelectric materials as transducers for wireless power transfer applications. The desired system would ideally demonstrate sufficient power efficiency and power output, with less mass by using piezoelectric materials as compared to cables as a means for power transfer. Piezoelectric materials, when used in this mode, are considerably less efficient means of power transfer as compared to cables and wires (Tseng et al., 2019), but they are useful in applications where a high electrical efficiency can be exchanged for enhanced mass efficiency. In military applications, as well as civilian applications, reduced mass can be useful in power transfer systems designed for flight and/or for orbit.

Optimization of wireless power transfer through the use of piezoelectric materials is advantageous for use in submarines, naval vessels, autonomous vehicles for land or marine use, and aircraft. These applications would be suitable for use in hazardous operating environments as wireless capabilities enhance safety as they bypass the requirement of physical access (Lawry et al., 2013). Additionally, the use of intersecting wires can become troublesome and unrealistic, especially in applications that require a covert nature (S. Lin et al., 2016). The penetration needed through a surface for a wired array can expose systems to vulnerabilities such as pressure loss, chemical leakage, and insufficient thermal or electrical insulation (Chang et al., 2007).

Additionally, the use of wires through materials can initiate undesired stress concentrations across the length of the wire that reduce structural stability (Chang et al., 2007). Wireless power transfer with piezoelectric materials could also be used to charge batteries in sealed areas (S. Lin et al., 2016), including applications of interest to future operations by NASA (Chang et al., 2007). The medical field could benefit from the optimization of this system in transferring power to implants that require power input (X. Wang et al., 2019), which can eliminate the need for replacement surgeries (Shahab & Erturk, 2014). When ambient vibrational energy is insufficiently available, wireless power transfer with piezoelectric materials can be used to supply power in applications that are unable to take advantage of the energy harvesting applications of piezoelectric materials (Allam et al., 2019).

Additionally, wireless power transfer can be used in power delivery to sensors for monitoring the structural health of airplanes (X. Wang et al., 2019), where the sensors may be placed in remote or obscure locations (Allam et al., 2019). The wireless powering of a permanent sensor network for aircraft could save time and money currently dedicated to conducting inspections as well as the potential for reduction in current aircraft design constraints (Monaco et al., 2015). The use of wires in the desired sensing network for aircraft is not suitable because of the increased weight and intricacy of a wired system (Kural et al., 2013). This wireless power transfer system could be even applied to powering sensors in hazardous locations such as spaces for nuclear waste storage (Shahab & Erturk, 2014).

To date, researchers at ARL have modeled and experimented with a system of piezoelectric transmitters and receivers. In the system tested experimentally, a piezoelectric transmitter mounted on an aluminum plate sent vibrations via Lamb waves, also known as ultrasonic guided plate waves (Tseng et al., 2019). Lamb waves are often used in Non-Destructive Evaluation (NDE) (Stobbe et al., 2019) for structural health monitoring (Giannelli et al., 2016). Lamb waves have several particle vibration modes, but the two major modes are the asymmetric mode and the symmetric mode (Aryan et al., 2014). They are named after British mathematician, Horace Lamb, to recognize the work he did in advancing the understanding of these waves and building off the work of Lord Rayeligh on guided wave propagation (Su & Ye, 2009). Lamb waves are applicable to wireless power transfer as they allow energy to be carried across the plate's length instead of through a metal, which allows for transmission to occur over greater distances (Tseng et al., 2019). This acoustic transmission as an option for wireless power transfer is especially advantageous in applications where Faraday shielding inhibits electromagnetic transmission through metallic materials (Lawry et al., 2013). Additionally, acoustic transmission through ultrasonic frequencies has demonstrated potential in improving the distance of transmission and minimizing losses of energy as compared to electromagnetic transmission methods (Shahab & Erturk, 2014). The use of acoustic transmission is also desired in medical applications where electromagnetic transmission is not appropriate (Shahab & Erturk, 2014).

In the system researched at ARL, actuation of the piezoelectric material patches convert the electrical energy into vibrations and the piezoelectric materials are used to subsequently transduce mechanical vibrations back into electrical power. This system employs both the direct and indirect piezoelectric effect. The indirect effect is observed at the piezoelectric transmitter when it is electrically excited to initiate the acoustic transmission. At the receiver, the direct piezoelectric effect allows for the conversion of the transmitted acoustical energy in the form of Lamb wave vibrations into electrical energy (S. Lin et al., 2016). The transmitter can be thought of as an "energy converter" and the receiver can be described as an "energy receiver" (X. Wang et al., 2019). Figure 3 illustrates this system.

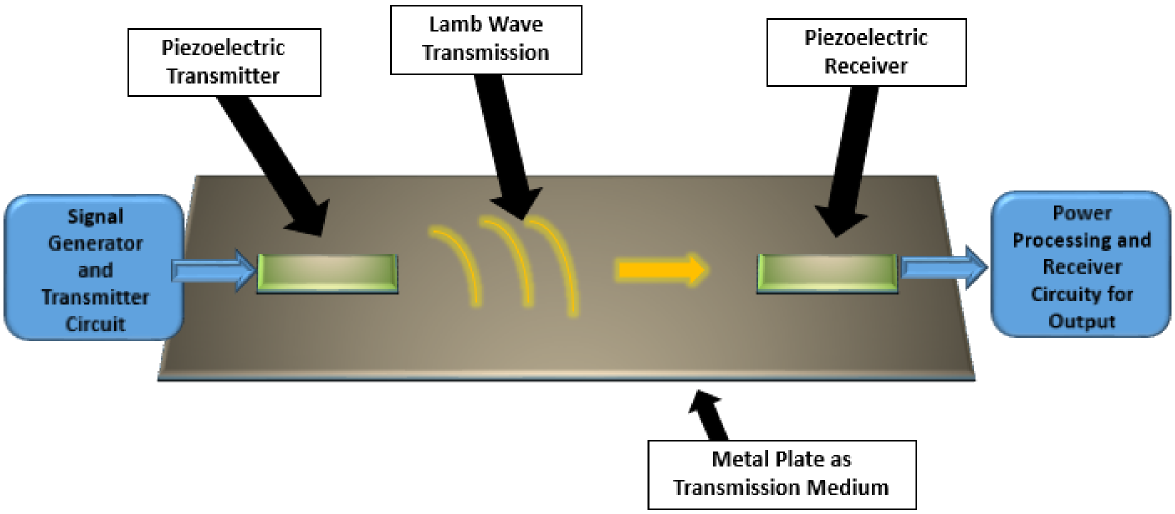

Figure 3: Model of system of interest with piezoelectric transmitter and receiver attached to a metal plate with vibrations via Lamb wave or guided plate waves transmission

This research has expanded on the current research of the team at the Army Research Laboratory by seeking optimal configurations for electrical transduction efficiency over ultrasonic excitation frequency ranges. To accomplish this optimization, a computational multiphysics model that captures the key physics was developed. This model was used to determine the ideal placement of the transducers on the structure, the frequencies over which these systems are their most responsive, and what combination of electrical, mechanical, and geometric parameters yield electrically efficient systems. Finally, the second semester goal of this project was to explore systems with multiple piezoelectric receivers on a device such that they could be selectively excited or "pinged" by a single transmitter. This allowed for the unique capability to excite a desired receiver without eliciting a significant response from the other undesired receivers while still achieving the required power efficiency for a given application.

Literature Review:

The following sections outline the relevant findings from a literature review on published research into piezoelectric materials. This includes the relative advantages and disadvantages of piezoelectric materials, past research findings on ways to improve power output, the importance of consideration of proper coupling mode, the results of research into different configurations and geometric structures, and electrical considerations.

Advantages and Disadvantages of Piezoelectric Materials

Piezoelectric materials are advantageous in some applications due to their cost effectiveness, availability and their ability to be fabricated on miniature scales that can be useful in various applications where space is limited. They also work well with electronic systems. Piezoelectric materials, because of their compact size, can be optimized for minimum weight, which is advantageous in applications when a low mass system is desired such as in aeronautic or astronautic applications (Juan et al., 2007). For these applications, piezoelectric composite materials, which are characterized by high stiffness-to-weight and high strength-to-weight ratios, have been developed due to improved methods of design and manufacturing (Liu et al., 1999). Piezoelectric materials are also relatively inexpensive. In their application as sensors, they are advantageous as they can quickly generate feedback (Liu et al., 1999), which is desirable for rapid structural health monitoring (Hameed et al., 2019) and their use as biosensors (Mahbub et al., 2017). They also have demonstrated large power output densities (Čeponis et al., 2019) and large voltage outputs (Cottone et al., 2012).

A potential disadvantage of piezoelectric materials is that their maximum effectiveness typically occurs over a relatively narrow bandwidth around the resonant frequencies of the parent structure/piezoelectric material system. This relatively narrow bandwidth can make operation in environments with variable environmental excitation frequencies more difficult and significantly less efficient (Chen et al., 2014). As such, when designing a system utilizing piezoelectric materials, it is necessary to consider the environment of operation as such an understanding sheds light on the range of possible excitation frequencies that may exist and properly tailor the piezoelectric material and parental structure resonant frequencies to these ranges (Adhikari et al., 2009). For the current research, given that the project is a transmission/reception application, it can be reasonably assumed that there is sufficient control of the excitation frequency.

Another disadvantage of piezoelectric materials is that the strain is not always distributed evenly across piezoelectric materials, which can result in varied performance (Čeponis et al., 2019) due to self-cancellation of the output voltages (Kural et al., 2013). Furthermore, piezoelectric ceramics are known to be relatively brittle (Freiman & White, 1995). Additionally, piezoelectric materials are sensitive to drastic changes in temperature, which can result in fluctuations in the natural frequency of the material (Zhou et al., 2013).

Researched Methods of Improving Power Output

Improving the total power output and efficiency are two of the central goals in research into piezoelectric materials as energy harvesters. In the current research, the piezoelectric materials are used as transducers. Means for improving harvesting capabilities are relevant to the current research as optimal transmission and reception can leverage the lessons learned from harvesting applications. For example, efficiencies greater than 80% have been obtained by some piezoelectric harvester cantilevers made of PZT when being used at their resonant frequency (Qi et al., 2010). This is relatively large for most piezoelectric systems as damping from the environment such as air often results in significant further losses in efficiency. In a recent publication, an efficiency of 56% was achieved with a system using piezoelectric materials as a transmitter and a receiver along a aluminum plate (Tseng et al., 2019). The losses in this case can be reasonably attributed to fluid-solid interaction as well as viscoelastic losses in the piezoelectric-to-structure adhesive layer.

Many other studies have been conducted to find various ways of increasing power output and overall efficiency. Past research that studied piezoelectric materials in a closed chamber found that the output voltage decreased in the presence of increasing pressure (Y. Wang et al., 2016). Increasing the thickness of the piezoelectric layer or adding additional layers of piezoelectric materials increases the power output (Hajati & Kim, 2011). Other research found maximum power output was achieved by reducing the mechanical damping across the piezoelectric harvester and increasing the electromechanical coupling (Adhikari et al., 2009). To measure the amount of electromechanical damping, an electromechanical coupling coefficient has been defined and relates how well the energy is converted from mechanical energy to electrical energy within a piezoelectric element. The electromechanical coupling coefficient is a useful metric in comparing different piezoelectric materials in their performance (Ramadan et al., 2014). This can be described as shown in Equation 1 and Equation 2.

$$S = s^{\epsilon}\sigma + d\epsilon \qquad (1)(\text{Jalili, 2010})$$
$$D = d\sigma + \beta^{\sigma}\epsilon \qquad (2)(\text{Jalili, 2010})$$

In Equation 1 and Equation 2, d represents the electromechanical coupling. Together these two equations relate the mechanical and electric fields for piezoelectric materials. S denotes the mechanical strain and s represents the compliance or the inverse of the material stiffness of the material. The applied mechanical stress is denoted by σ. D is dielectric displacement and β represents the absolute dielectric permittivity of the medium. ϵ is the electrical field strength. The ϵ, when used as a superscript, indicates the compliance is measured when the electric field is constant or zero. The superscript, σ, indicates β is determined when the load is constant or zero (Jalili, 2010).

Research by Michael I. Friswell and Sondipon Adhikari also found that the shape and size of piezoelectric harvesters (PEH) can have a significant effect on power output. The shapes they studied are illustrated in Figure 4 (Friswell & Adhikari, 2010).

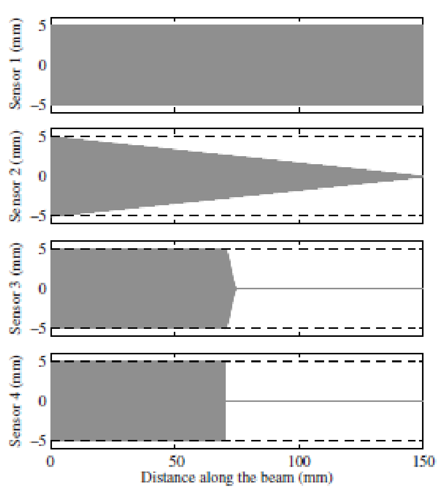

Figure 4: Varying Shapes of Sensors Studied by Friswell and Adhikari (Friswell & Adhikari, 2010)

This study found that the capacitance of the PEH decreases as the length of the PEH decreases and the coupling coefficient increases (or becomes less negative as they defined the coefficient). This resulted in an increase in the power output of the PEH. Their results demonstrating this trend can be seen in Table 1 (Friswell & Adhikari, 2010).

Table 1: Results of Study on Effect of Shape and Size of Harvester on Capacitance, Electromechanical Coupling, and Power Output (Friswell & Adhikari, 2010)

Sensor number	Description	Capacitance (pF)	Coupling	Power output (W)	
				Full model	Single mode
1	Uniform	44.27	−0.00918	6.361	6.549
2	Triangular	22.14	−0.00667	10.17	10.76
3	Segment (smooth)	21.40	−0.00762	13.48	13.80
4	Segment (square)	20.66	−0.00748	13.65	13.98

Research by Young K. Hong and Kee S. Moon found improved power output with single crystal relaxor ferroelectric material (PMN-PT) with the use of interdigitated electrode (IDE) design (Hong & Moon, 2005). PMN-PT has significantly larger piezoelectric coefficients and electromechanical coupling factor than PZT. PMN-PT is a single crystal, meaning that its resonant behavior is more consistent with the understanding that the overall resonant behavior is a combination of the piezoelectric element and the parent structure. This consistency combined with the larger piezoelectric coefficients and coupling factor make PMN-PT a viable alternative to PZT for improving power output. The IDE design is illustrated in Figure 5. This design can be achieved by photolithographic processes during fabrication and has been found to produce open circuit voltages 20 to 30 times larger than the conventional normal plane design due to a larger induced electric field. (Hong & Moon, 2005).

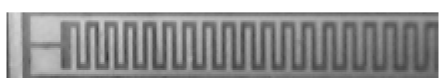

Figure 5: Illustration of Sample with Interdigital Electrode Design (Hong & Moon, 2005)

Importance of Consideration of Proper Coupling Mode

When designing systems with piezoelectric materials, it is important to be aware of what piezoelectric coupling mode is best suited for the desired application. The two most common modes are the longitudinal and transverse modes (Saadon & Sidek, 2011). The longitudinal or 33 mode occurs when the electric polarization of the piezoelectric and the applied stress share a common direction. The piezoelectric d_{33} coefficient refers to this longitudinal mode. The transverse or 31 mode refers to the case when the polarization is generated perpendicular to the load applied. For the transverse mode, the d_{31} coefficient is used (Ramadan et al., 2014). The differences between these modes are illustrated in Figure 6.

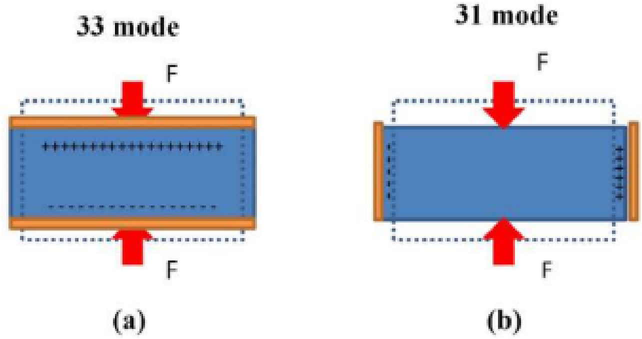

Figure 6: The Longitudinal (33 mode) and Transverse (31 mode) for Piezoelectric Materials (Ramadan et al., 2014)

Different Configurations and Geometrical Structures

In addition to considering the proper coupling mode for the piezoelectric material, the configuration of the piezoelectric system and the overall geometry can also be considered when seeking ways to maximize efficiency and power output. For example, some possible configurations include the uni-morph and bimorph cantilever beams. Several studies have demonstrated that the uni-morph configuration is preferred for applications where the excitation frequency is low (Saadon & Sidek, 2011). For the bimorph cantilever beam, one can attach the piezoelectric patches in series or parallel. A series bimorph cantilever configuration is optimal when excitation frequencies are large in magnitude. This configuration will result in a larger impedance across the piezoelectric device and is optimal configuration under high loads. The parallel connection results in maximum power output in environments with medium excitation frequencies. These different configurations are illustrated in Figure 7 (Saadon & Sidek, 2011).

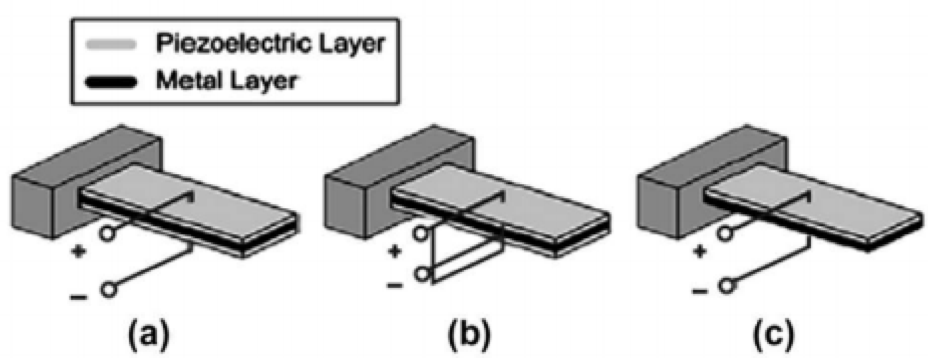

Figure 7: Illustrations of Various Configurations: (a) Series bimorph, (b) Parallel bimorph, (c) Unimorph cantilever (Saadon & Sidek, 2011)

In addition to varying the piezoelectric material configurations, one can vary the structural geometry of the system to maximize power output. Traditionally, a rectangular shaped cantilever beam is used due to its simplicity and demonstrated success in energy harvesting. For improved operation, other shapes have been proposed such as triangular shaped, trapezoidal shaped, and even 'cymbal' shaped cantilever beams. An example of a 'cymbal' shaped beam is illustrated in Figure 8. Past research found the triangular shape allowed for larger deflections and thus larger power outputs than a traditional cantilever. Studies using trapezoidal shaped beams found that this structure allowed for a more even distribution of strain throughout the entire system and a significantly larger energy output (Saadon & Sidek, 2011).

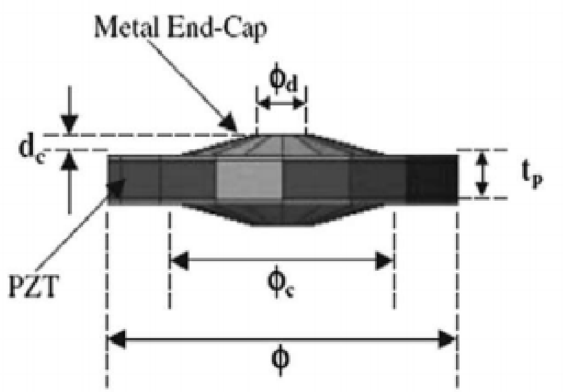

Figure 8: Illustration of 'cymbal' shaped cantilever structure (Saadon & Sidek, 2011)

Receiver Circuitry

When using piezoelectric materials to collect and transduce ambient vibrational energy, it is essential to design and optimize receiver circuitry to ensure the generated electrical power is in a useful form (Howells, 2009). Often this electrical receiver circuit uses a system of zener diodes to rectify the current output that is an initially alternating current (Z. L. Wang et al., 2009) into a DC output for battery storage. This process is outlined in the block diagram in Figure 9. A capacitor is also useful in storing the energy as it is collected from ambient vibrations. The capacitor will discharge the voltage to a load once a specific level of voltage is met by the capacitor (Howells, 2009).

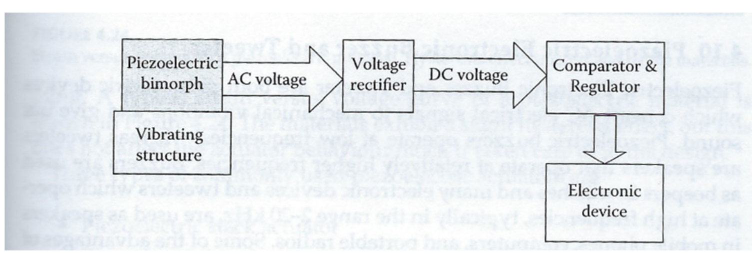

Figure 9: Block Diagram Describing Piezoelectric System for Energy Harvesting (Vijaya, 2013)

In addition to the need for a rectifier to convert the output current from AC to DC, a DC-DC converter is often implemented for storage and regulation of energy that is harvested. An inductor can be used to ensure the energy from the piezoelectric harvester is transferred at specific points in the cycle of vibrations, but this can be difficult to successfully accomplish due to timing issues (Sankman & Ma, 2015).

It has also been demonstrated that the use of a load inductor in parallel to the piezoelectric element and resistor used in the electrical circuit for a piezoelectric transducer can improve the overall electrical efficiency and power transduced (Tseng et al., 2019). With the load inductor, a recent study successfully increased power efficiency from 36% to 56%. The inductor helped to improve efficiency as it "rings out" the capacitive impedance of the receiving piezoelectric element (Tseng et al., 2019). The use of an inductor was also studied by (Adhikari et al., 2009) and by (Friswell & Adhikari, 2010). Schematics of two example circuits with and without an inductor for harvesting applications are shown in Figure 10 (Adhikari et al., 2009).

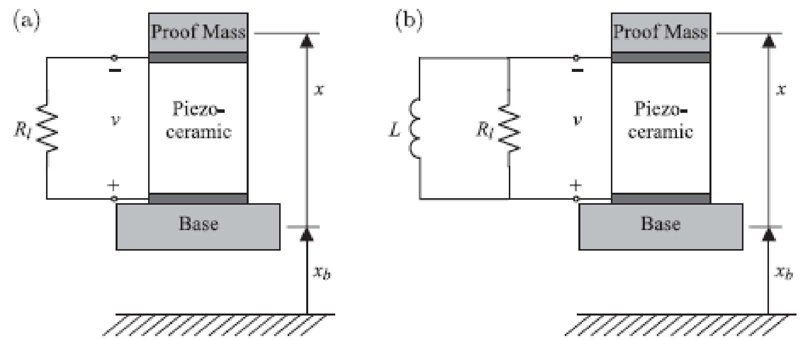

Figure 10: Schematics of Two Harvesting circuits, one without an inductor (a) and one with an inductor (b) (Adhikari et al., 2009)

Trident Research Methodology

The Trident project was divided into three main parts. First, a computational model of the single transmitter/receiver configuration on a metal plate was developed. This computational model was validated through comparison to existing hardware and published experimental results. Second, using this computation model, parametric studies of electrical transduction efficiency versus the array of electrical, mechanical, and geometric parameters were performed for a single piezoelectric transmitter/receiver pair. These studies were instrumental in determining what parameters were most significant in the performance of the system. Third, using the results of this parametric study, a single transmitter/receiver article of the system was experimentally tested. Finally, the project concluded with developing a model of a power transfer system with a single transmitter/multiple receiver array to selectively excite a specifically targeted receiver.

Computational Model

A COMSOL Multiphysics model was developed for the electromechanical transduction system described above. Figure 11 outlines some of the capabilities of COMSOL Multiphysics that make it an advantageous and desirable software to employ.

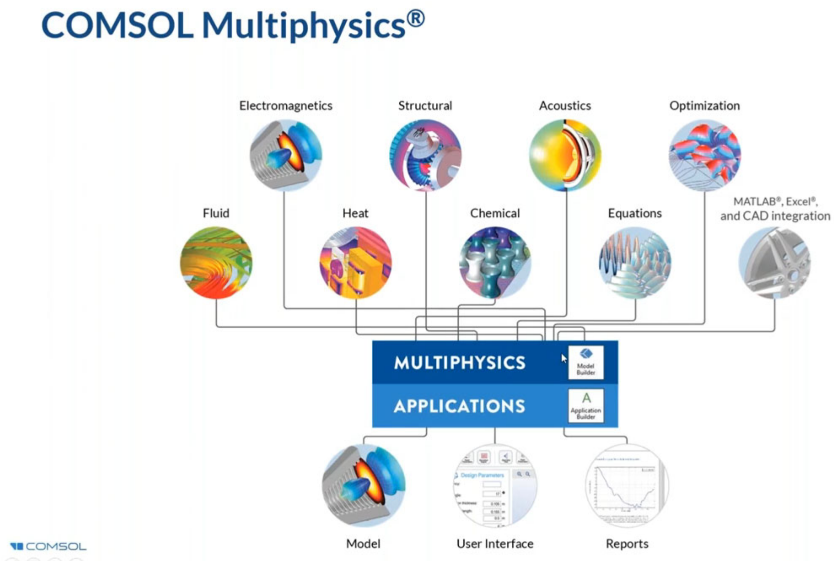

Figure 11: Illustration of COMSOL Capabilities (*18-Minute Introduction to COMSOL Multiphysics*®, n.d.)

The relevant physics included are: solid mechanics, electrostatics, piezoelectrics, ACDC circuits, viscoelasticity, and structural acoustic/acoustic emission. This was accomplished by 3D modeling the geometry, discretizing the structure, imposing all the relevant loads, properties, and boundary conditions, and numerically solving the resulting fully-coupled nonlinear system. Modal analysis was first performed to determine what resonant frequencies exist over the frequency range of interest. The model was swept over the frequency domain of interest and the electrical transduction efficiency was analyzed. These sweeps were performed with particular attention paid to the area in the vicinity of the resonant frequencies.

Significant progress towards the creation of an accurate COMSOL model that quantitatively captures experimental results had been made by Tseng et. al., however, the developed model required non-physically based correction factors to match the experimental results, which will be discussed later in more detail. The computational model that has been developed was compared with the above cited experimental results for validation. Figure 12 illustrates the preliminary success the ARL team has had in composing a simpler COMSOL model that matches experimental performance.

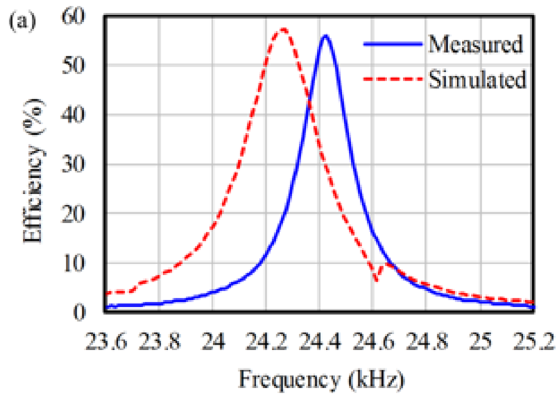

Figure 12: COMSOL Multiphysics Model Comparison (Tseng et al., 2019)

In Figure 12, the red dashed line represents the efficiency vs frequency plot predicted from COMSOL and the blue line represents the plot determined from measurements taken during an experimental analysis of a single piezoelectric transmitter/receiver pair mounted on an aluminum plate. The experiment used Macro-Fiber Composite (MFC) transducers, a compensation inductor ring, and DP460 as a bonding material (Tseng et al., 2019). Similar plots were used in analyzing and understanding the accuracy of the computational results in COMSOL. Again, it must be noted that the model published by Tseng et. al., includes several non-physically based correction factors to get the model to match the experiment.

To improve upon this model, more attention was dedicated to understanding the physical reasons behind the losses of energy through the medium. In the previous model, these losses were accounted for after experimental validation by adding non-physical material damping to the structural metal. These properties were determined based on the experimental analysis instead of the relevant physics acting within the system. By furthering the analysis and detail of the adhesive layer within the model, the relevant physics behind the energy losses were captured more realistically. Previous work forewent considering the viscoelastic adhesive layer and the acoustic emission at the fluid/solid boundaries that significantly influence the acoustic transmission.

The refinement of the computational model was not a trivial step, but the work leveraged recent advancements in an accurate model’s development. It is important to note that the present work focused on modeling the system of piezoelectric transducers for a plate. The focus on plate geometry allowed for capturing of the necessary physics considerations within COMSOL with the goal of using the model for optimization of the system of interest. The use of COMSOL has been advantageous as it allowed for modeling of specific 3D geometry as illustrated by Figure 13.

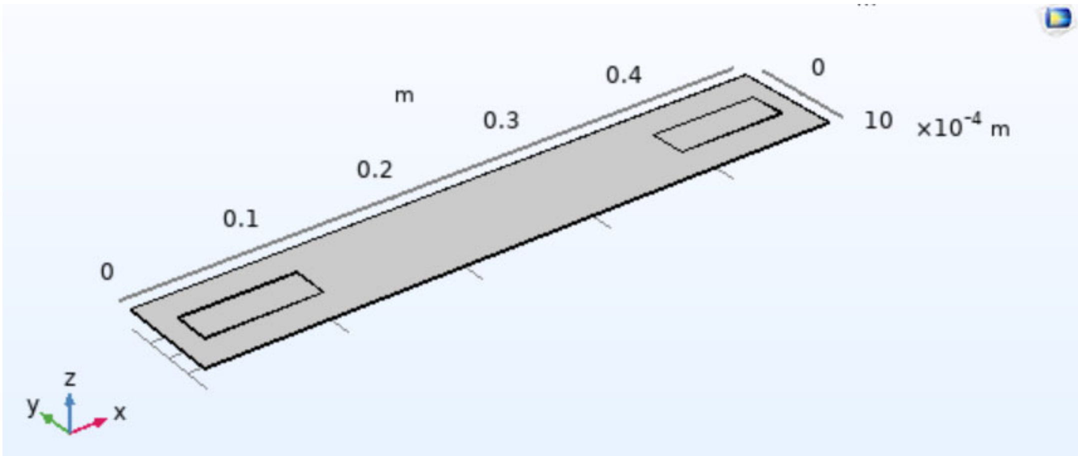

Figure 13: Illustration of the Capability of COMSOL to model desired 3D Geometries from the developed model

In the computational modeling, the geometric considerations built off those used by the team at ARL. The values used in the computation model are outlined in Table 2.

Table 2: Dimensions for Computational Modeling of the System of Interest (Tseng et al., 2019)

Geometric Consideration:	Anticipated Numerical Value:
Piezoelectric transducer area	85mm x 28mm 85mm x 14mm 56mm x 28mm
5052 Aluminum Alloy Plate	80mm x 480mm x 0.8mm
Distance between transducers	277mm
Inner edge of transmitter	16.7mm from aluminum plate edge

These specific dimensions of the developed model were compared to the experimental results obtained by the ARL team (Tseng et al., 2019). This comparison allowed for validation and refinement of the developed computational model.

In addition to the capability of modeling 3D geometries, mesh modeling within COMSOL is advantageous in composing an accurate model of the system of interest. Mesh modeling allowed for discretization of the system into finite elements and then the composition of a model that meshed or combined all of these necessary considerations. An illustration of mesh modeling from the developed model is included in Figure 14.

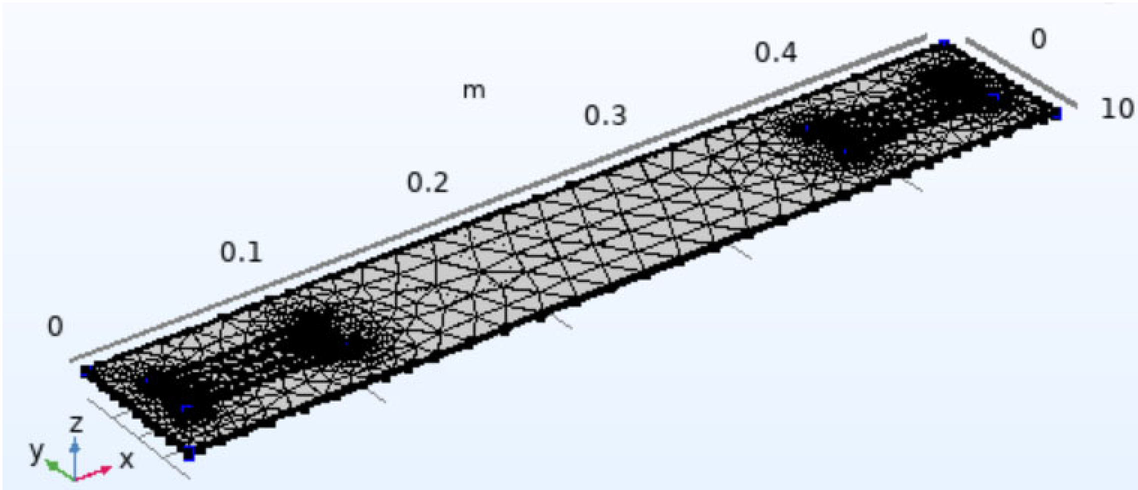

Figure 14: Illustration of Mesh Modeling within COMSOL from the Developed Model

The considerations for this mesh model included only meshing the solid components of the system. The significant portions of the acoustic emission that occur at the surface were sufficiently considered by using boundary elements with the mesh modeling in COMSOL. It was unnecessary to further account for the acoustic emission as the remaining portions that go into the void are not significantly impacting the system of study. The boundary conditions included zero displacement at a single point and rigid body motion suppression. This ensured the numerical values do not extend to unreasonably large values without unnecessarily limiting the strain field. The material properties were considered by using standards of COMSOL. Within COMSOL, the electric power and receiver circuits were similar to those of Tseng et al. and the adhesive properties were built off the findings of a paper published on epoxy polymers (Sideridis et al., 2006). The modeling of the adhesive layer was important in accounting for the viscoelastic behavior present in this layer that impacts the vibrations of the Lamb waves through the medium. This modeling aided in understanding the resulting dissipation of energy due to the adhesive layer.

The relevant COMSOL modules and models are outlined in Figure 15. The considerations of the physics modules were coupled with the multiphysics models (QIU et al., 2019). Together, these considerations allowed for the use of the mesh modeling to conduct frequency domain studies. Through a frequency domain study, the system was swept at varying frequencies with a focus on studying the efficiency or the ratio of power output to power input.

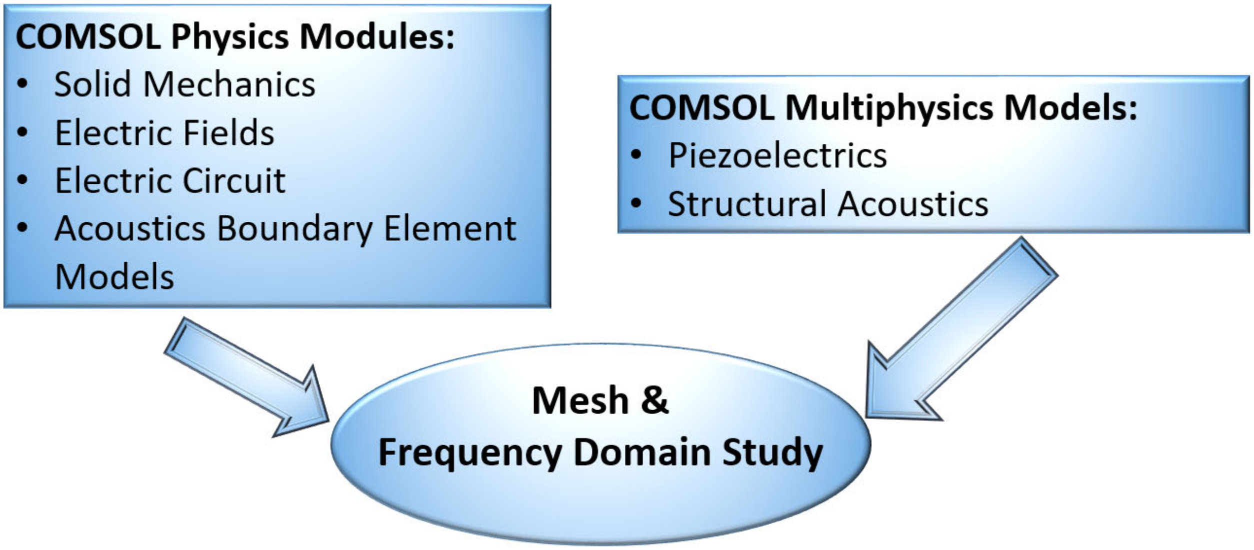

Figure 15: Outline of Relevant COMSOL Physics Modules and Multiphysics Models

Figure 16 illustrates the results of the computational model developed through the outlined methodology. Figure 16 illustrates the locations the developed model predicts peak efficiencies will occur and the magnitude of those peak efficiencies.

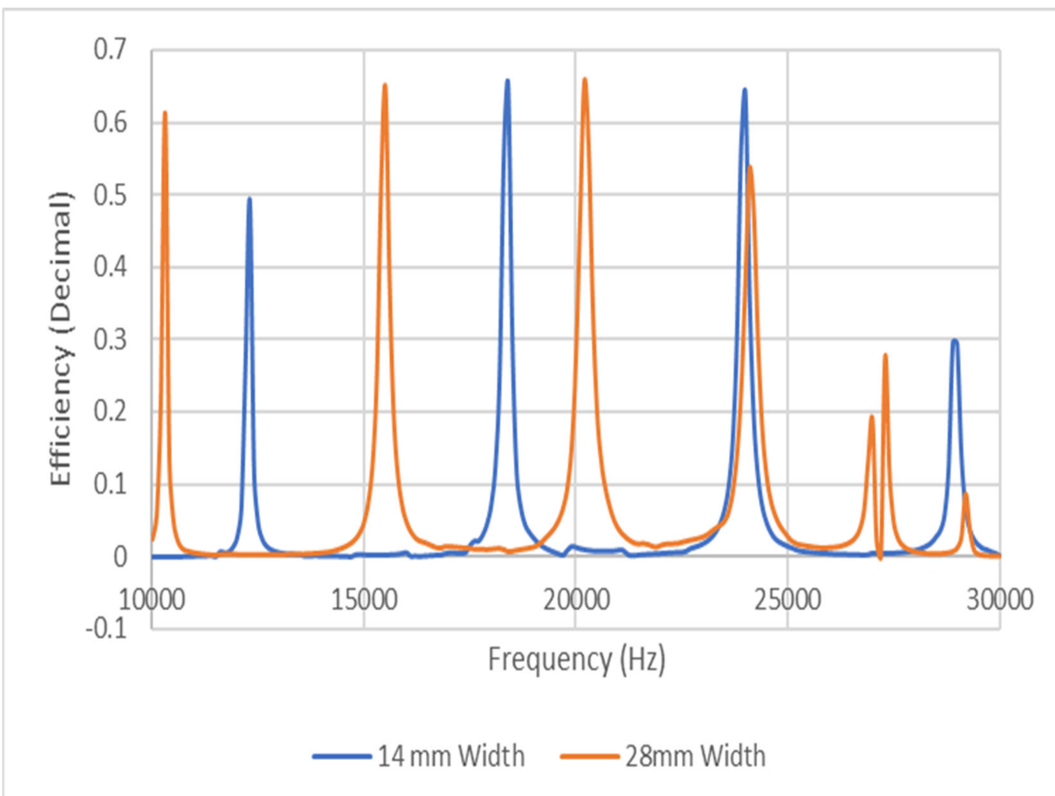

Figure 16: Results of the COMSOL Model for a Frequency sweep from 10kHz to 26kHz with 28mm Patch Width and 14mm Patch Width

Figure 16 illustrates a shift in the specific frequencies where the peaks in efficiency occurred when the width of the piezoelectric patch was adjusted. Additionally, there is a slight increase in the magnitude of the peak efficiencies in power transmission from the 14mm width case to the 28mm width case. This is most likely due to the fact that the increase in width doubles the active area of excitation for the piezoelectric patch.

The ARL team studied computationally and experimentally a system with piezoelectric patches with width of 14mm. Figure 17 displays the computational and experimental results from the ARL Team (Radice, 2020). The developed model used a width of 28mm to match the piezoelectric patch ordered for experimental analysis. Model validation occurred by comparing the results of the developed model in Figure 16 for the 14mm width case to the computational and experimental results from the ARL model for the 14mm width case. This comparison was a critical step in the validation of the developed COMSOL model.

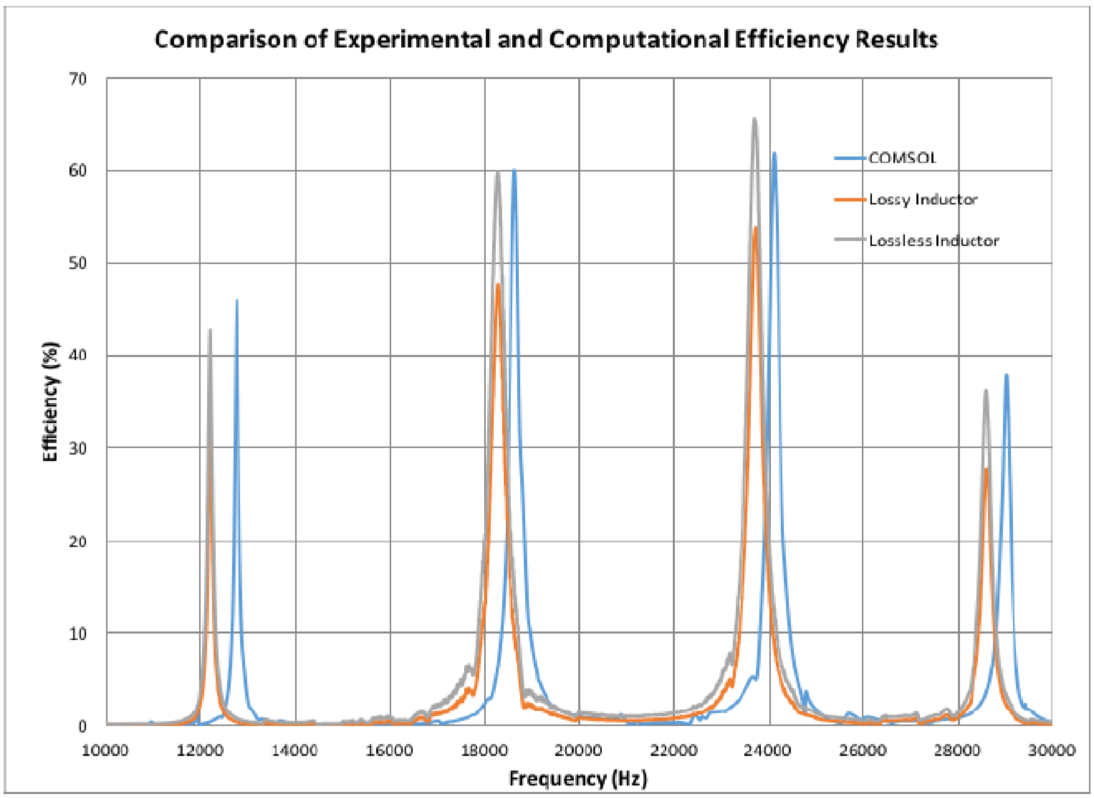

Figure 17: Computational Results of the ARL Team COMSOL Model with a width of 14 mm and Experimental Results from the ARL Team (Radice et. al)

A narrowed in example of the results for a frequency domain study using the developed model is illustrated in Figure 18. For this study, the system was swept at a range of frequencies from 14kHz to 16.4kHz with a step value of 10Hz. Across this sweep of frequencies, the efficiency or the ratio of the power output to power input was computed.

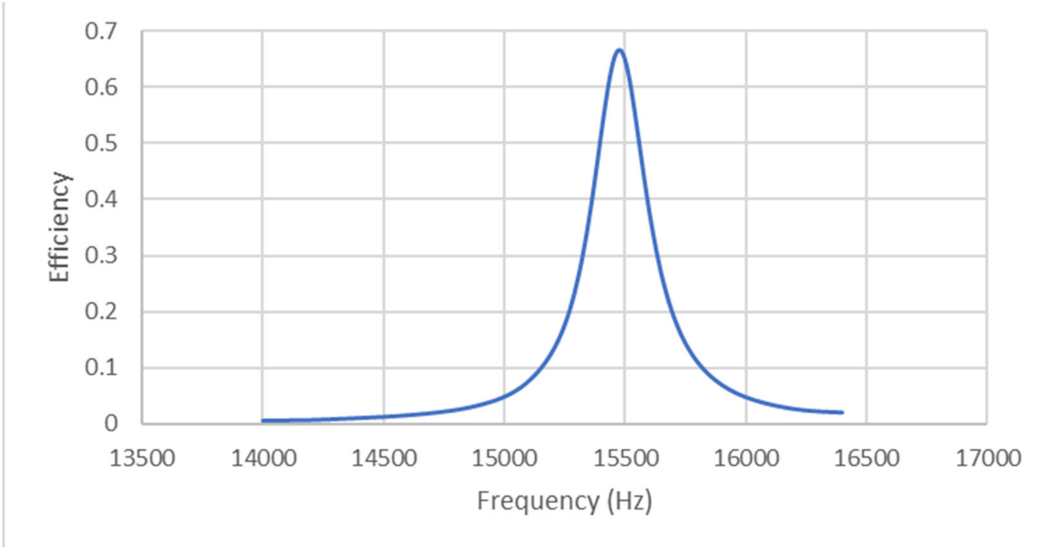

Figure 18: Illustration of a Frequency Domain Study with the Developed Model from 14kHz to 16.4 kHz

Figure 18 illustrates COMSOL's utility and flexibility in being able to conduct more detailed frequency sweep studies, which assisted in the refinement of the model.

After the initial model development, a model in COMSOL was developed with patches that had interdigitation as illustrated in Figure 19. Figure 19 illustrates the difference in modeling between a monolithic patch without interdigitation and a patch modeled with interdigitation. The interdigitation was modeled by alternating the direction assigned to the piezoelectric effect for each adjacent component of the patch within COMSOL. The model also included an inductor on the receiver side of the model. The purpose of the inductor was to ring out the inherent capacitance of the interdigitated piezoelectric device (Tseng et al., 2019). In previous models without interdigitation, the inductor was not necessary and therefore was not implemented.

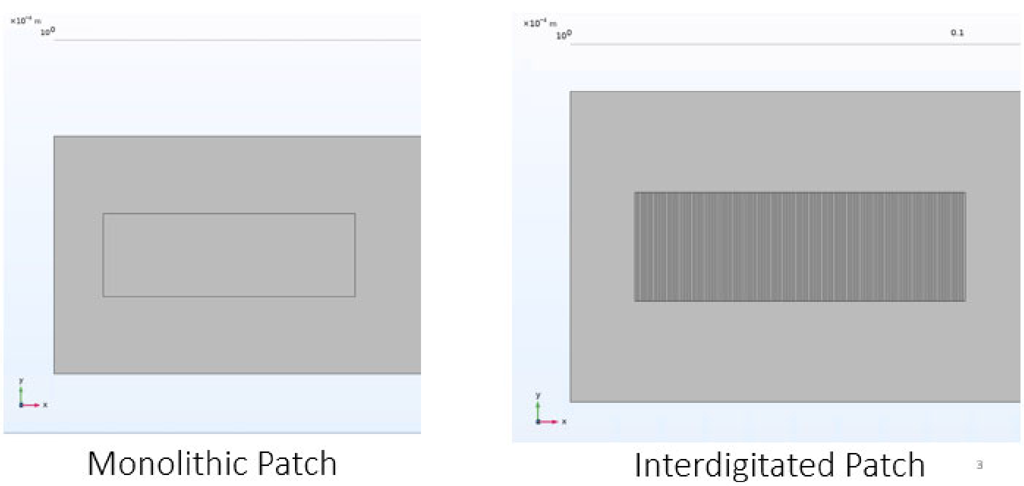

Figure 19: Comparison of Model Developed in COMSOL with a Monolithic Patch without Interdigitation and Model Developed in COMSOL with Interdigitation

Figure 20 offers a comparison of the mesh developed for a monolithic patch without interdigitation and a patch modeled with interdigitation, Interdigitation allows for a higher density of piezoelectric material within a piezoelectric transducer and has demonstrated desired effects, such as larger power outputs (Hong & Moon, 2005). Figure 20 illustrates that the mesh modeling of the interdigitated model is greater in complexity than the monolithic patch and it is expected that the computation time for models produced with interdigitation will be significantly longer than models without interdigitation.

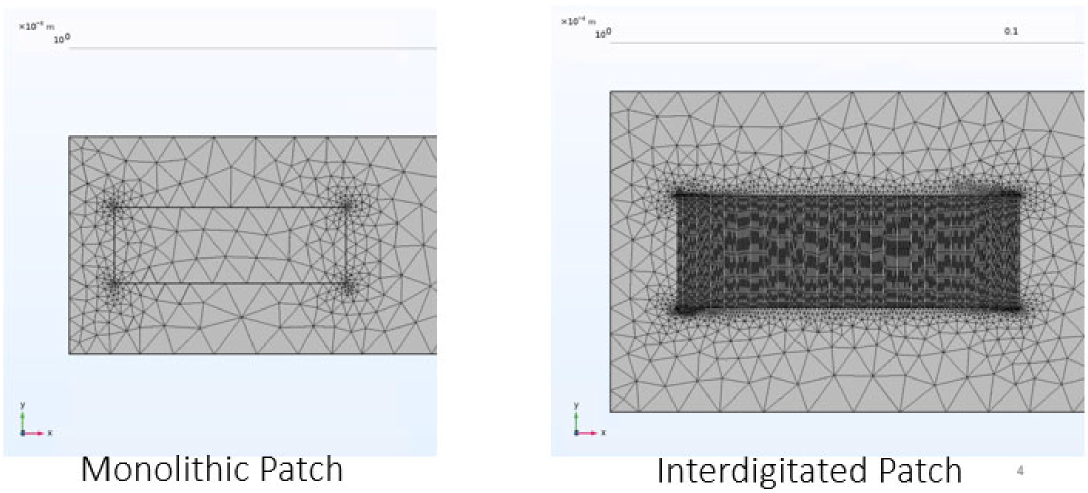

Figure 20: Comparison of Mesh of Monolithic Piezoelectric Transmitter Patch without Interdigitation and Piezoelectric Transmitter Patch with Interdigitation

Figure 21 illustrates the results of a frequency sweep from 10kHz to 30kHz using the interdigitated model with an inductor of 0.5 Henry's on the receiver side and a model without interdigitation.

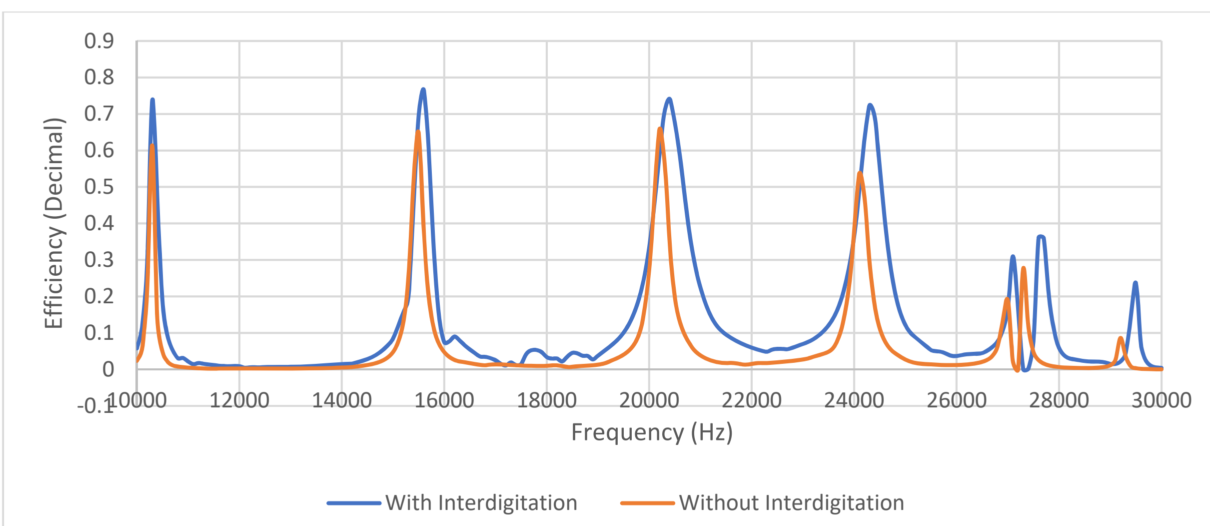

Figure 21: Efficiency vs Frequency for Model with Interdigitation and Inductor of 0.5 H

Figure 21 illustrates that modeling of the system with interdigitation and an inductor closely resembles the results of the modeling of the system without interdigitation and an inductor. It is important to note that the processing time significantly increased with the use of interdigitation as the interdigitated model increased geometric complexity that COMSOL had to process when running a study with finite element analysis. On average studies without interdigitation took about 14 hours to complete, while the interdigitation study took about seven days to complete. The system of interest in real world applications uses interdigitated piezoelectric patches. Figure 21 illustrates that studying a system of an interdigitated system can be practically done without explicitly modeling the interdigitation to achieve reasonable study and processing times within COMSOL. For the remainder of the Trident project, models produced did not include the explicit interdigitation within COMSOL, but instead modeled a system of interdigitated patches with the practical implementation of a system with rectangular patches assigned the piezoelectric effect and the absence of an inductor.

Parametric Study

The parametric study outlined below was performed using the developed COMSOL Multiphysics model. Table 3 outlines the parameters of study that have been taken into consideration:

Table 3: Parameters of Study Sorted by Category for Computational Parametric Study

Piezoelectric Material Properties	**Piezoelectric Element Configuration**	**Receiver Circuitry**	**Adhesive Layer Parameters**	**Other Considerations**
Relative permittivity	*Length*	*Inductance*	**Thickness**	**Material of Parent Structure**
Piezoelectric constant	*Width*	*Resistance*	**Material used/Modulus**	**Symmetry vs Asymmetry (bending or axial waves)**
Elastic modulus	*Thickness*	*Capacitance*		**Spacing between piezoelectric elements**
	Shape of piezoelectric			

In Table 3, the italicized section refers to the parameters that change collectively as the transducer used changes. They are included in the table as recognition that they are important considerations for the system of study, but these specific, italicized parameters were not changed on an individual basis. The parametric study focused specifically on the five bolded parameters and finding the optimal combination of parameters that maximized electrical transduction efficiency over the range of excitation frequencies of interest.

Computational parametric modeling following this approach allowed for a better understanding of the parameters, how they can be changed, and their influence on the overall system and performance and optimal efficiency without significant financial expense.

The parametric study on varying thicknesses of the adhesive layer considered thicknesses of 15 µm, 35 µm, 100 µm, and 1000 µm. The results are illustrated in Figure 22.

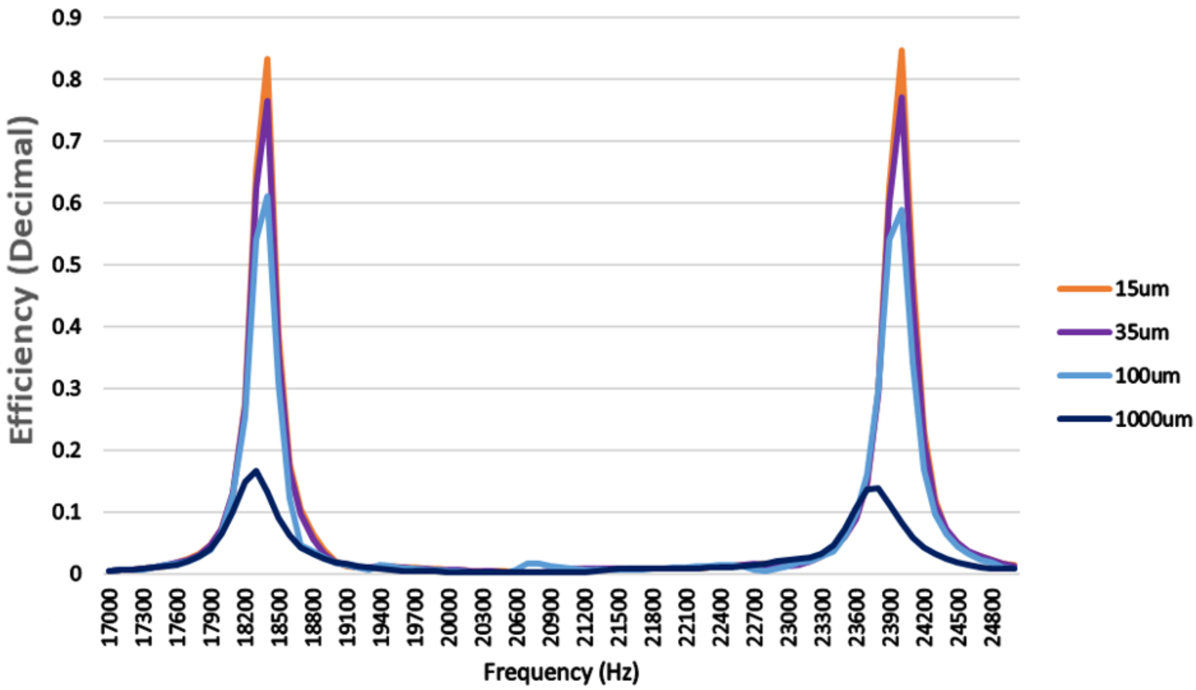

Figure 22: Results of the Parametric Study Analyzing Efficiency vs Frequency for Varying Thickness of the Adhesive Layer

Figure 22 illustrates that the thinnest adhesive layer experiences the highest peak efficiencies across the frequency sweep. The thickest adhesive layer of 1000 µm experiences the lowest peak efficiencies. This is due to the adhesive layer being a lossy material. With a thicker adhesive layer, a larger portion of the mechanical energy is absorbed by the adhesive layer instead of vibrating across the plate to be received by the piezoelectric receiver.

The parametric study analyzing varying the modulus of the parent material considered moduli of 190 GPa to 240 GPa. The results of this parametric study are included in Figure 23.

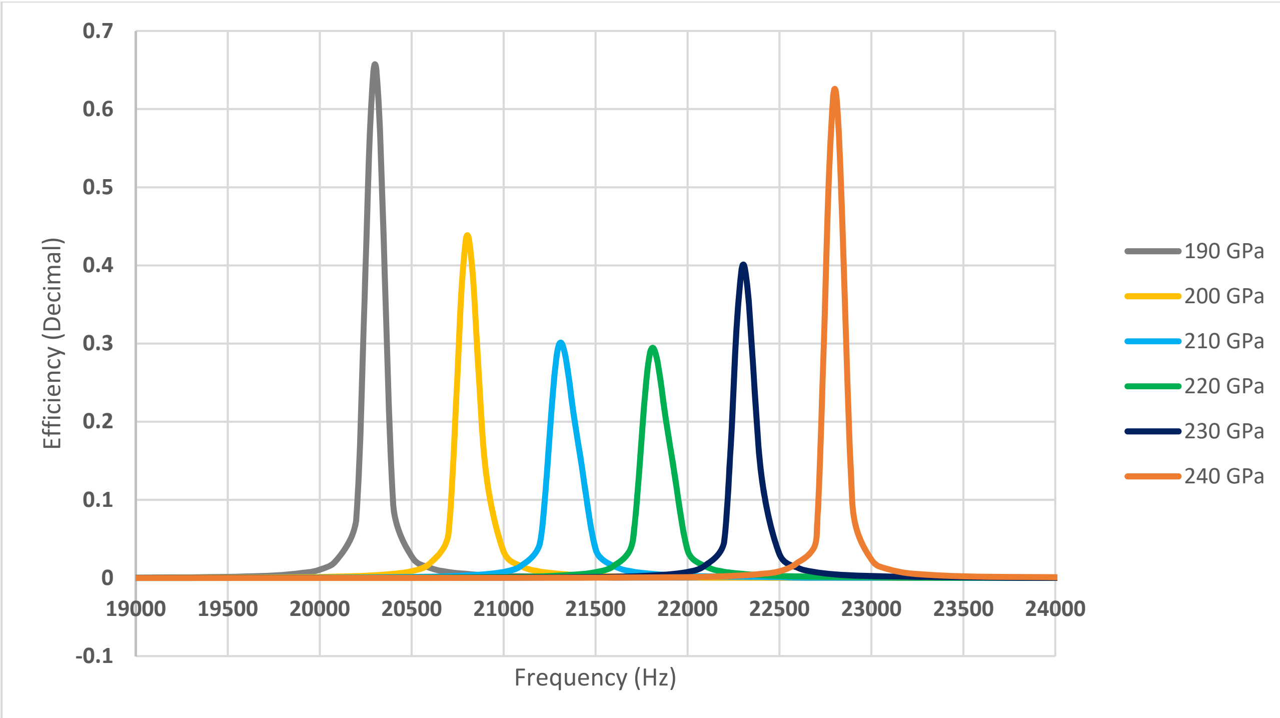

Figure 23: Results of the Parametric Study Analyzing Efficiency vs Frequency for Varying Modulus of the Parent Material

Figure 23 illustrates that as the modulus changes, the magnitude and location of the peak efficiency experienced by the system changes.

Following investigation into the varying of the modulus of the parent material, the modulus of the adhesive layer was also studied. Figure 24 illustrates the results of a computational study that varied the real and complex parts of the modulus of the adhesive layer. The study was conducted in the frequency range of 23kHz to 25kHz.

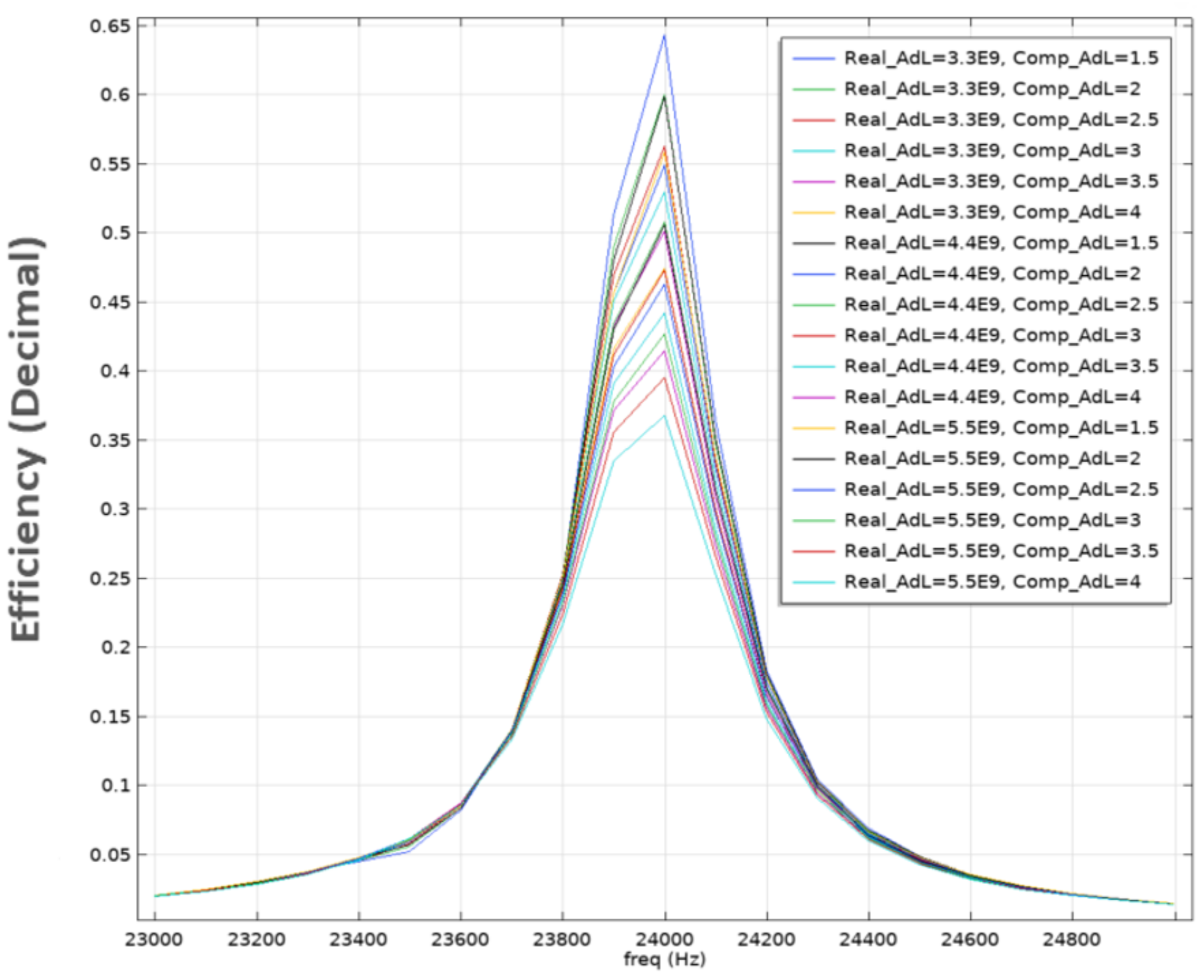

Figure 24: Results of the Computational Parametric Study Analyzing Efficiency (Decimal) vs Frequency (kHz) for Varying the Real and Complex Parts of the Adhesive Layer

The use of a complex valued modulus for the adhesive layer allows for capture of viscoelastic losses of the vibrations from the piezoelectric patch through the adhesive layer into the parent material (Radice et al., 2020). This parametric study specifically studied varying the tensile modulus of the adhesive layer, but it is important to note that the shear modulus and Poisson's ratio will all have complex components if the tensile modulus does (Radice et al., 2020). Figure 24 illustrates that the smaller the magnitude of the real and complex parts of the tensile modulus, the higher the efficiencies that result. The highest efficiency of about 64% was achieved with a tensile modulus of 3.3E9 + 1.5j Pa, while the lowest efficiency of about 36% was achieved with a tensile modulus of 5.5E9 + 4j Pa. As the tensile modulus increased in magnitude, the adhesive became more lossy and thus dissipated more of the vibrations from the piezoelectric material into the environment, which drove down the efficiency.

Following the study into the modulus of the adhesive layer, symmetric vs asymmetric systems were studied.

Figure 25 illustrates the system developed in COMSOL to analyze power transfer using a symmetric system with piezoelectric patches mounted on both sides of the plate for axial wave transfer. Prior asymmetric models with piezoelectric patches mounted on only one side of the plate had analyzed power transfer using flexural and axial waves. To initiate power transfer with the goal of suppressing the transfer of flexural waves a second pair of piezoelectric patches were placed on the bottom of the plate directly below the first pair of piezoelectric patches to develop the symmetric system. Suppression of flexural waves is desired as they contribute to some of the losses experienced by the system as they cause lateral deflection of the system. In prior asymmetric models, the power transfer occurred through axial waves and symmetric or bending waves, which have flexural waves.

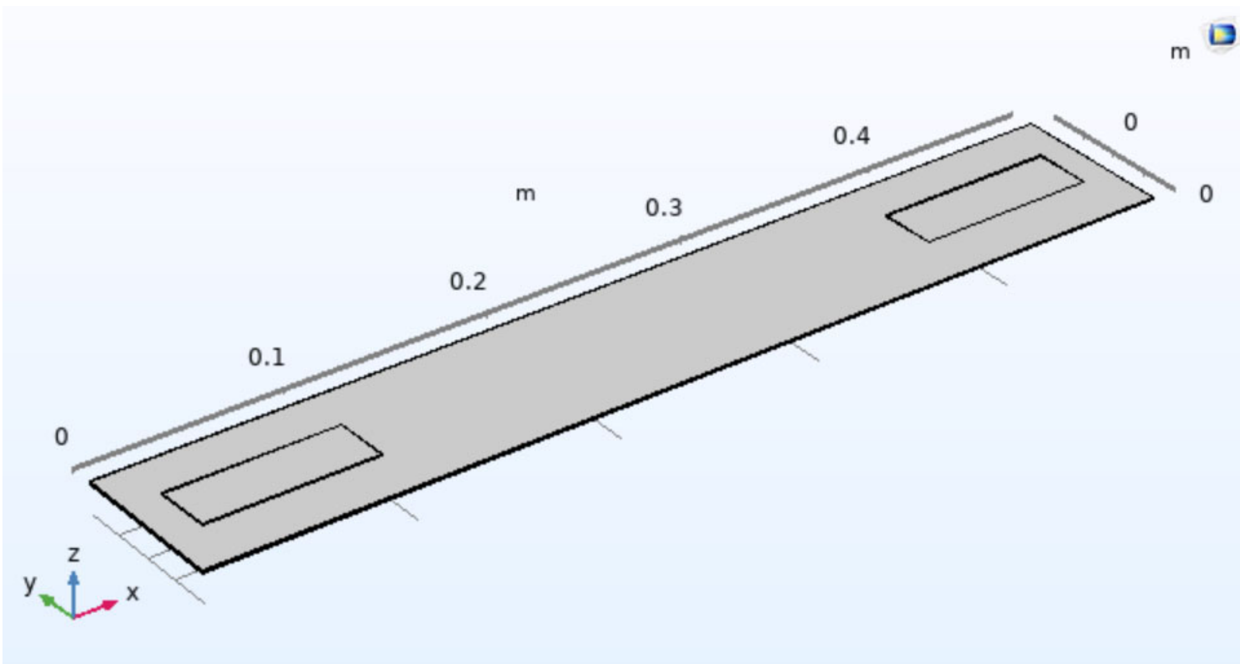

Figure 25: Top Side of Schematic of Symmetric System Developed for Power Transfer Using Axial Waves

Figure 25 illustrates the top side of the system developed for axial wave power transfer through the use of two pairs of piezoelectric patches. In Figure 26, the bottom side of the plate is illustrated with the second pair of piezoelectric patches.

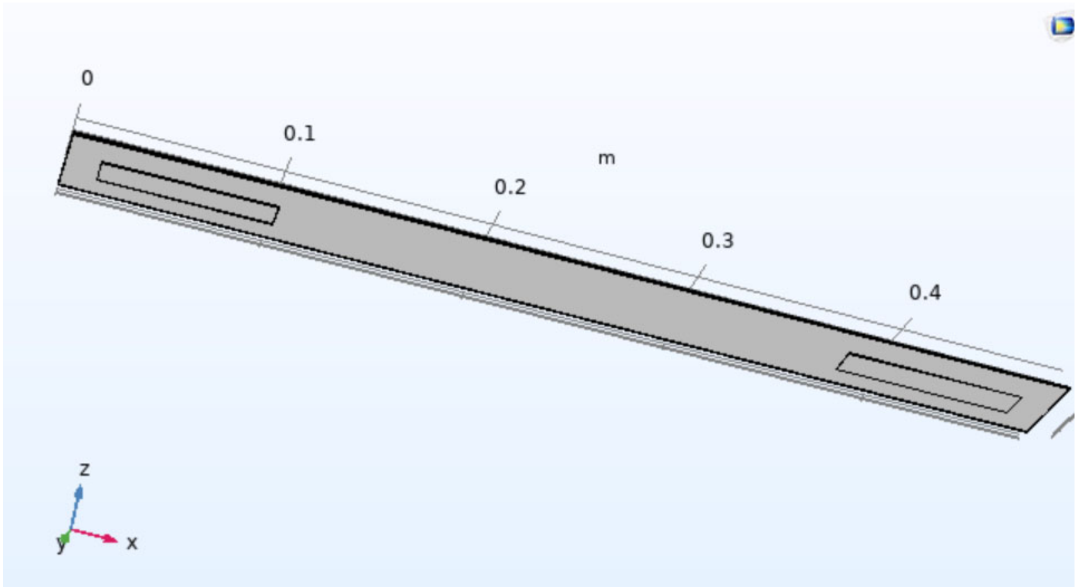

Figure 26: Reverse Side of Schematic of Symmetric System Developed for Power Transfer Using Axial Waves

Figure 27 illustrates the wireframe of the schematic for the system studying axial wave power transfer. Figure 27 illustrates the two pairs of piezoelectric patches used to eliminate the flexural wave and decrease lateral deflection. The wireframe view of Figure 27 allows the two pairs of piezoelectric patches to be visible.

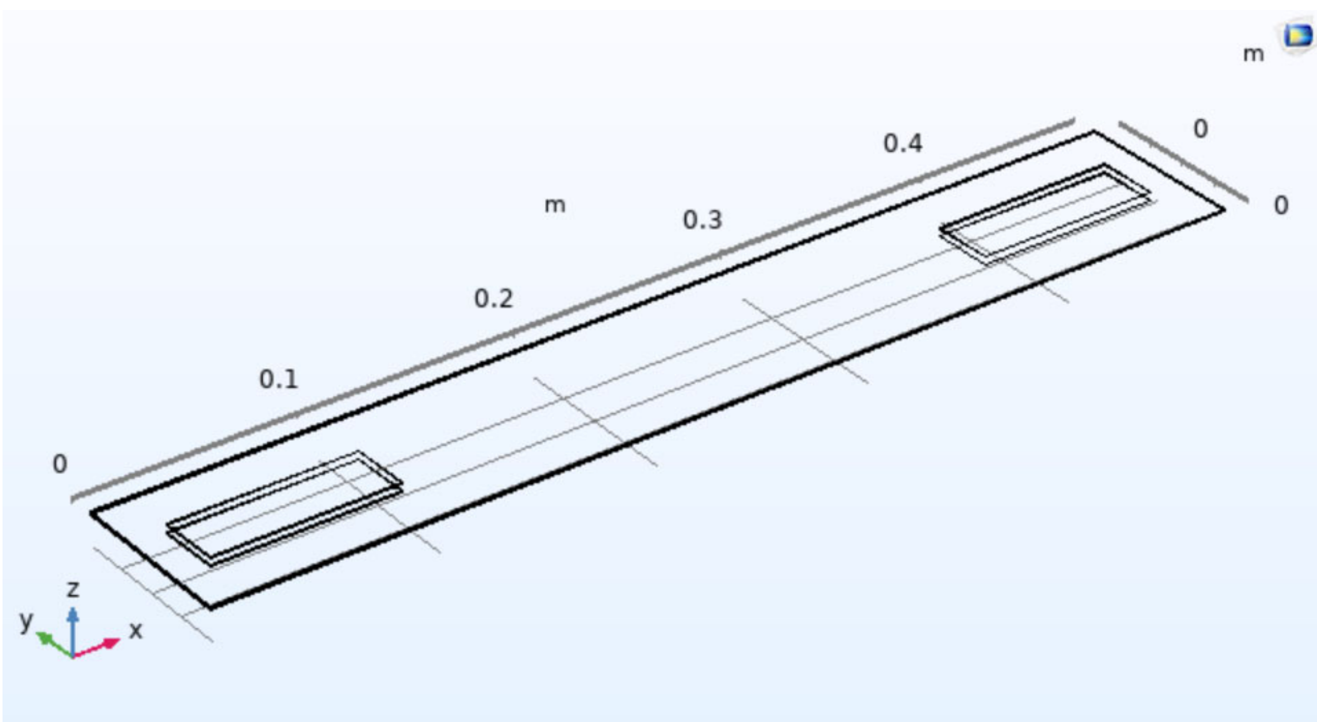

Figure 27: Wireframe of the Schematic for the Symmetric System Studying Axial Wave Power Transfer

A frequency sweep was conducted for the symmetric system using axial wave power transfer and compared to a frequency sweep done for the asymmetric system that had both axial and flexural wave power transfer. Figure 28 illustrates the results of the frequency sweeps.

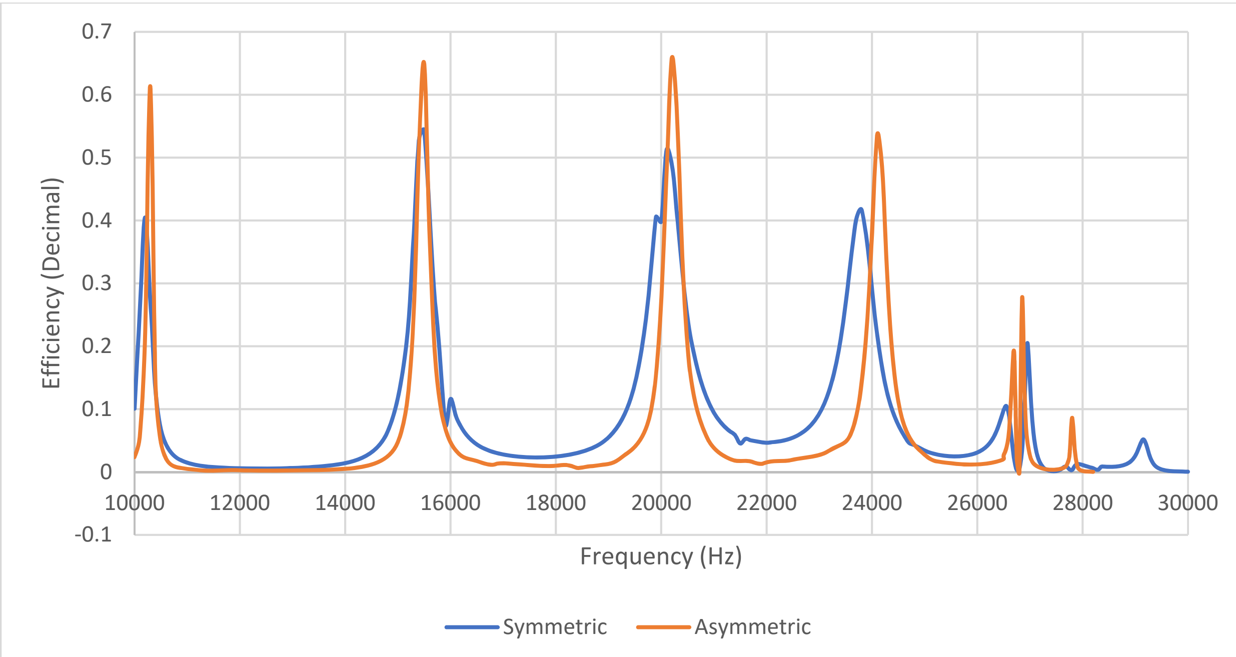

Figure 28: Comparison of Results for Frequency Sweeps Using the Asymmetric System vs Symmetric System

Figure 28 illustrates that the elimination of the flexural waves through the use of two pairs of piezoelectric patches resulted in a broader peak at the excited frequencies. A broader peak is desired in applications where one may not have as much control of the input excitation frequency. It was expected that the magnitude of the peak efficiencies would increase with the symmetric system. This is an area of future work as further studies with finer sweeps and meshes will enhance the understanding of the performance of the symmetric system.

The final computational parametric study analyzed varying the spacing between piezoelectric elements. Figure 29 illustrates the original spacing used where the piezoelectric patches were spaced 0.277m apart.

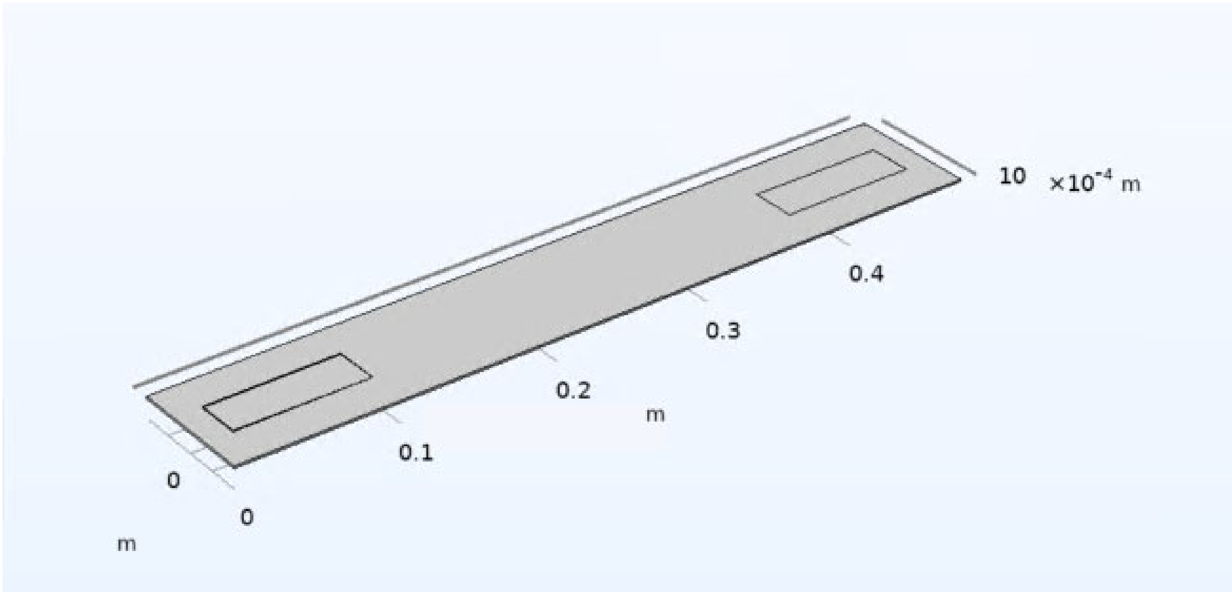

Figure 29: Original Spacing of 0.277m between the Two Patches

Figure 30 illustrates the spacing for two models developed with smaller spacing, one with 0.1m and the other with 0.2m between piezoelectric elements.

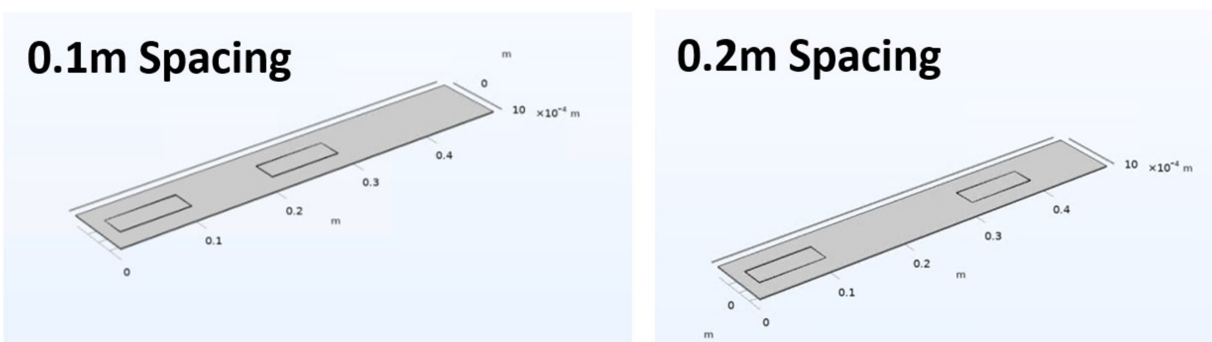

Figure 30: Models Developed with Smaller Spacing than that of the Original Model with 0.277m between the Two Patches

Figure 31 illustrates the comparison of the results for each model, the 0.1m spacing, the 0.2m spacing and the 0.277m spacing.

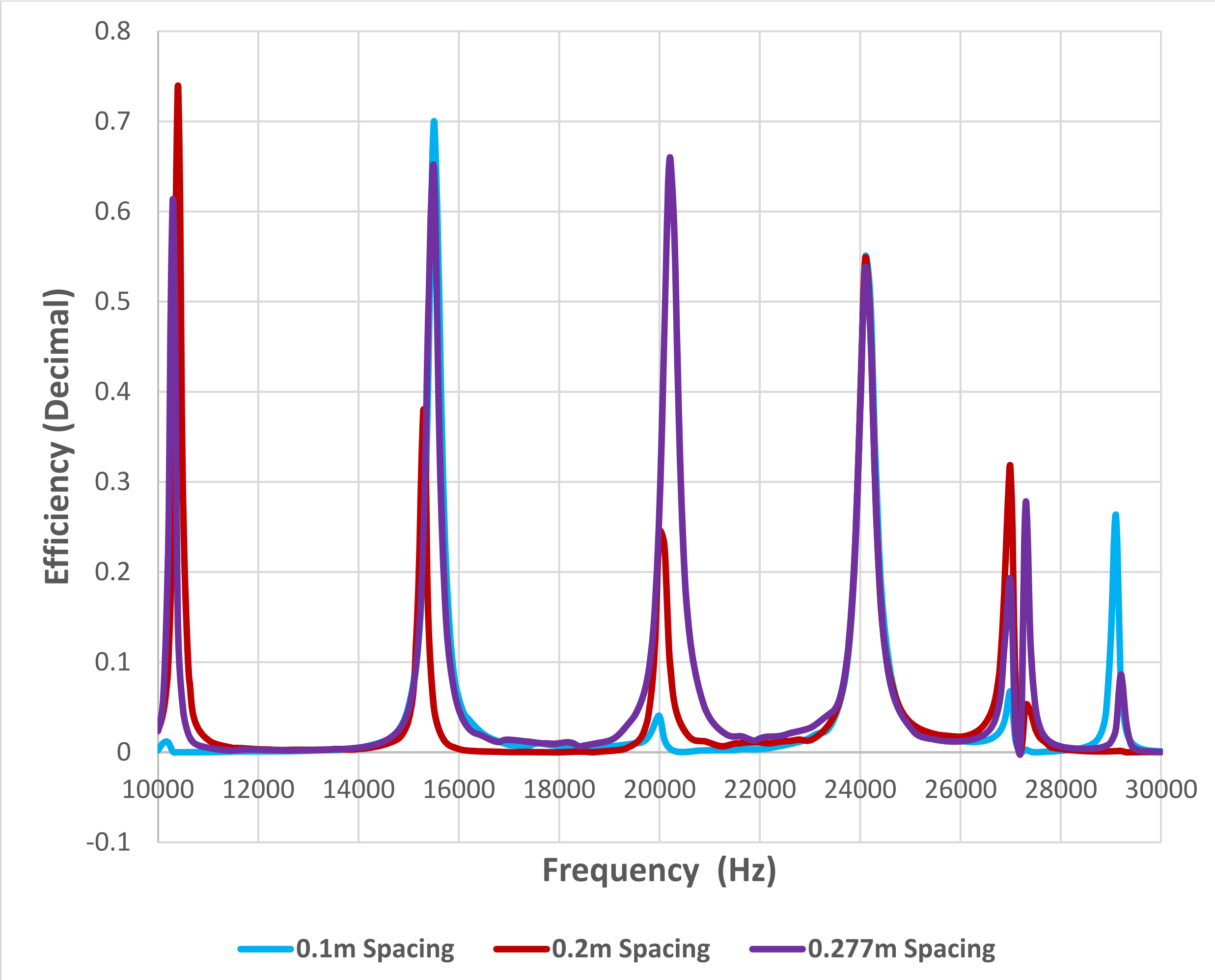

Figure 31: Comparison of Results for 0.1m of Spacing, 0.2m of Spacing, and 0.277m of Spacing Between Piezoelectric Elements

Figure 31 illustrates that the original spacing of 0.277m resulted in the largest number of peaks of significant magnitude. The model with 0.1m spacing did have a slightly higher peak at about 15.5 kHz and 29 kHz, but did not have any other peaks significantly higher than the model with 0.277m spacing. The model with 0.2m spacing did have a slightly higher peak at about 10.4 kHz and 27 kHz, but did not have any other peaks significantly higher than the model with 0.277m spacing.

Figure 32 illustrates the spacing for two models developed with larger spacing than the original 0.277m spaced model, one with 0.4 m and the other with 0.577 m between piezoelectric elements.

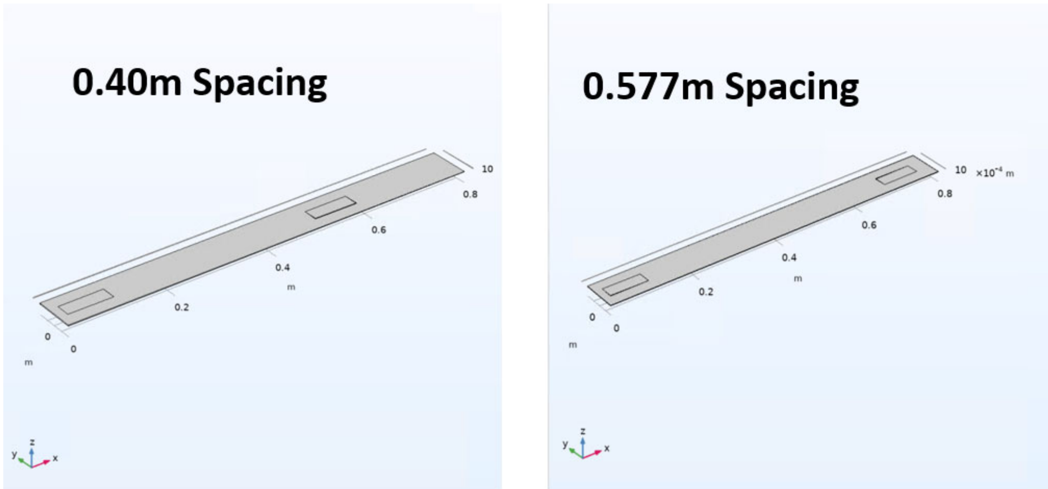

Figure 32: Models Developed with Larger Spacing than that of the Original Model with 0.277m between the Two Patches

Figure 33 illustrates the comparison of the results for each model, the 0.4m spacing, the 0.277m spacing and the 0.577m spacing.

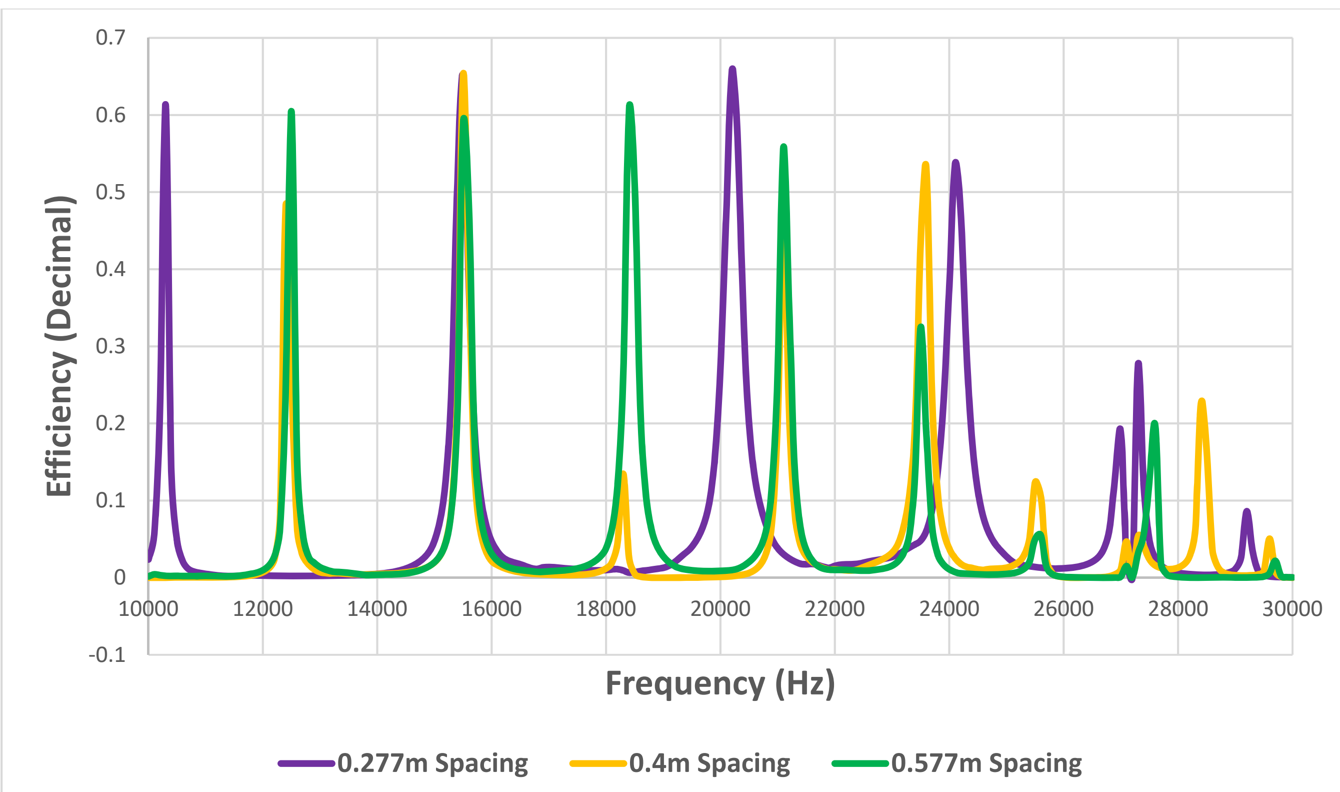

Figure 33: Comparison of Results for 0.4m of Spacing, 0.277m of Spacing, and 0.577m of Spacing Between Piezoelectric Elements

Figure 33 illustrates that there is a slight shift in the frequencies of interest where the patches are most excited as the patches become more spaced out. For example, the model with 0.277m of spacing achieved a peak at about 10kHz, while the models with 0.4m and 0.577m achieved a comparable peak at 12.5 kHz. Figure 33 illustrates that the larger spacing produced results more comparable both in number of peaks and magnitude of peaks to the original spacing of 0.277m than the smaller spacing did as illustrated in Figure 31. The smaller spacing did produce peaks in more similar locations to the original spacing of 0.277m as noted by the shift of peak frequencies illustrated in Figure 33 for larger spacing.

Figure 34 illustrates a final comparison for the results from all five models with varying spacing.

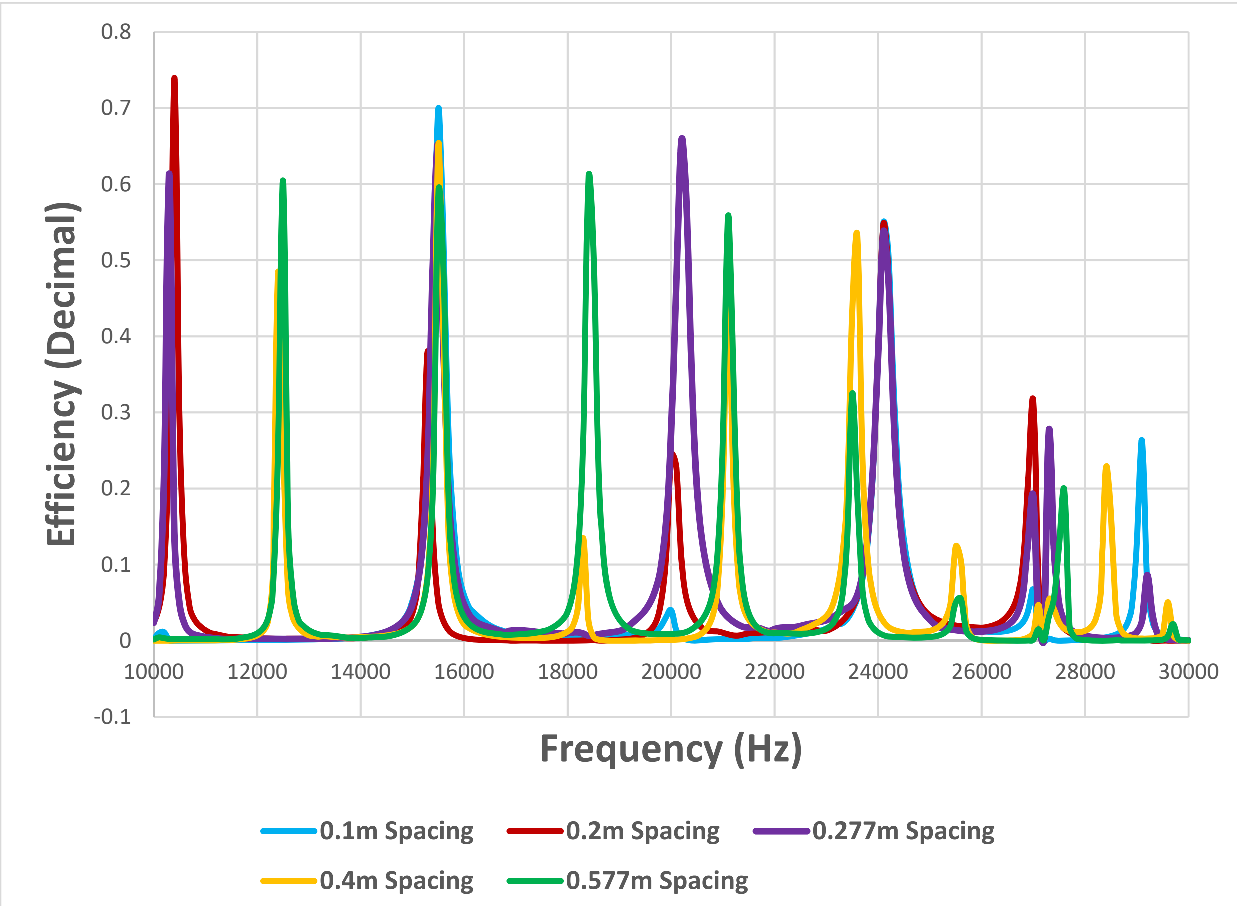

Figure 34: Comparison of Frequency Sweep Results for Varying Spacing for Models with 0.1m, 0.2m, 0.277m, 0.4m, and 0.577m of Spacing Between Piezoelectric Elements

Figure 34 illustrates that the largest number of peaks with magnitude above 40% efficient occurred for the models with spacing greater than 0.277m spacing. The models with 0.1m and 0.2m of spacing did exhibit one frequency where they achieved efficiencies past 60%, but the large majority of their peaks fell below 40%.

Experimental Work

Due to several quarantines in which restrictions were placed on access and time in the lab, the experimental phase of the originally proposed project was not fully completed. The experimental work conducted drew from conclusions reached from the parametric studies. The experimental analysis revealed environmental factors that were not initially included in the model and improved understanding of the application of piezoelectric materials to real-world applications.

The outline of the experimental process is to measure the transduction efficiency of the device swept over the frequency range of interest. The transduction efficiency can be understood to be the ratio of output power over input power and ranges from 0% to 100%. Equation 3 illustrates this calculation.

$$Efficiency = \frac{Power\ output}{Power\ input} * 100 \qquad (3)$$ (Chang et al., 2007)

The experimental analysis was accomplished in a relatively straightforward way by capturing the input voltage, the input current, the phase lag between them, and repeating the same for the output voltage, current and phase lag. For the AC signals considered here, the input power, the output power, and electrical transduction efficiencies can then be calculated.

It is important to note that the primary focus was on optimizing the values of electrical efficiency. The values for voltage and power output were considered and analyzed, but in optimizing wireless power transfer, electrical efficiency is more critical in quantifying the success of a system (S. Lin et al., 2016).

These experiments were conducted with standard circuit laboratory equipment that was available at USNA. An initial experimental setup was completed in Rickover Hall and final analysis occurred with resources available in Hopper Hall. Initially, Vaseline was used as the adhesive material as a temporary solution to allow for initial experimental testing as the Vaseline allowed for temporary placement of the piezoelectric actuators. Vaseline is an extremely lossy material and the measured efficiencies were extremely low in magnitude. The piezoelectric materials were eventually bonded to the plate using Crystalbond 555. Crystalbond is not as lossy of a material as Vaseline and allows for a somewhat temporary bonding as it can be melted down. The initial experimental setup using Vaseline is illustrated in Figure 35.

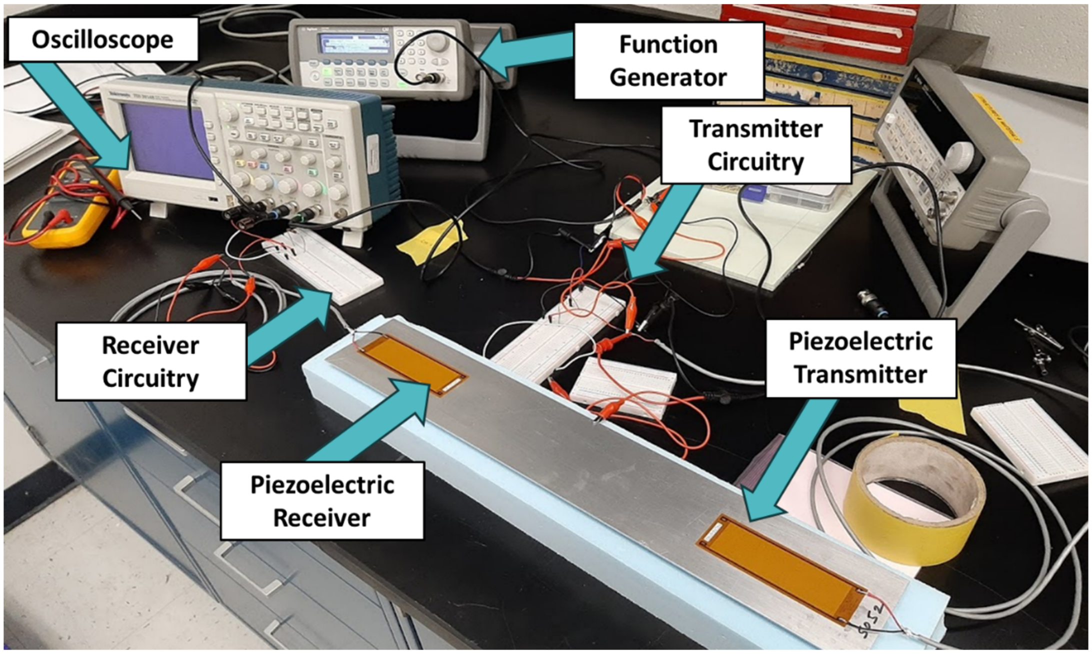

Figure 35: Initial Experimental Setup

The equipment included using a function generator to excite the piezoelectric transmitter and initiate the Lamb wave transmission (Lawry et al., 2013). Figure 36 illustrates a function generator.

Figure 36: Function Generator

The excitation frequencies and voltages were adjusted with this generator (S. Lin et al., 2016). Power amplifiers have been used in past systems (Lawry et al., 2013), but are not necessary when focusing on studying the efficiency of transmission (S. Lin et al., 2016). An oscilloscope was used to determine the input and output voltages of the system (Chang et al., 2007). Figure 37 illustrates an oscilloscope.

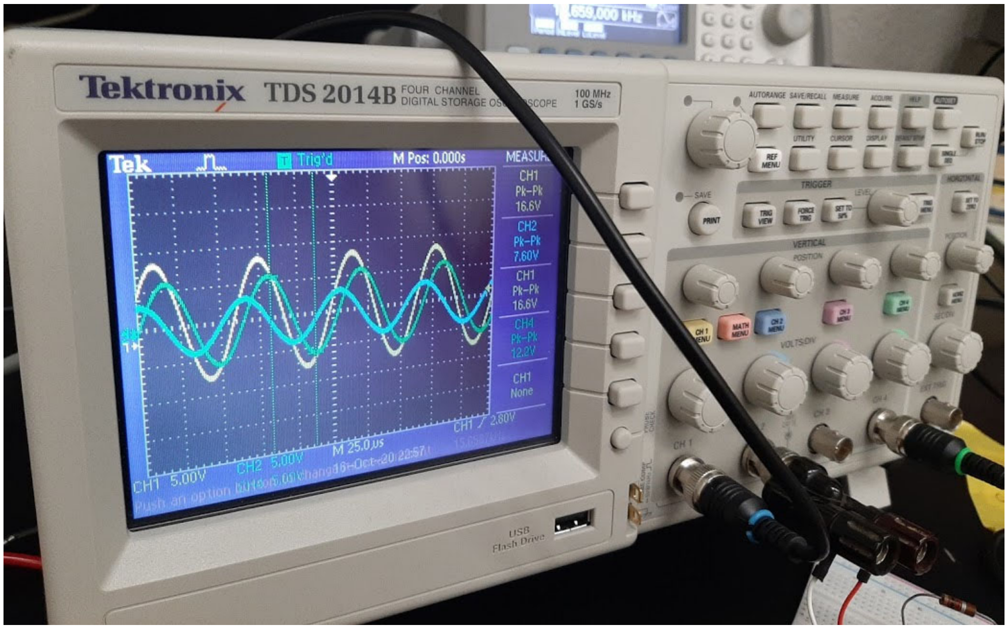

Figure 37: Oscilloscope

In the initial setup, the transmitter and receiver circuitries each included a resistor in series with the respective piezoelectric patch. The resistor values were known and could be experimentally measured through the use of a digital multimer. Three voltage measurements were taken across the system. The voltage across the piezoelectric transmitter and the voltage across the resistor in series with the piezoelectric transmitter were measured and multiplied together. This product was multiplied by the current to determine the power input according to Equation 4. The current was calculated by dividing the measured voltage across the transmitter resistor by the known resistance. The final voltage measurement was taken across the piezoelectric receiver. This voltage was multiplied by the current to calculate the output power according to Equation 4.

The power was calculated by using Equation 4. I_{rms} is the value of the output alternating current and R_{load} is the resistance of the load used (Elfrink et al., 2009).

$$P = I^2{}_{rms} * R_{load} = VI \qquad (4) \text{ (Elfrink et al., 2009)}$$

The power outputs are less than one watt for the system of interest. Because of this low power value, it is not necessary to consider significant heating of the adhesive layer or the transmission medium within the model.

A modified experimental setup was developed that better allowed for power calculations. On the transmitter side, the piezoelectric patch was connected to a Bode Vector Network Analyzer that excited the patch with a known voltage. A current probe on the transmitter side allowed for the complex measurement of the current. The product of the voltage and the conjugate of the current allows for the determination of the input power. On the receiver side, the piezoelectric material was connected to a circuit with a load resistor and inductor. An oscilloscope was used to measure the voltage across the piezoelectric material and the resistance of the load resistor was known. To calculate the output power, the square of the voltage across the receiver piezoelectric material was divided by the known resistance of the resistor.

Figure 38 illustrates the updated setup to the experimental analysis using the Bode Vector Network Analysis.

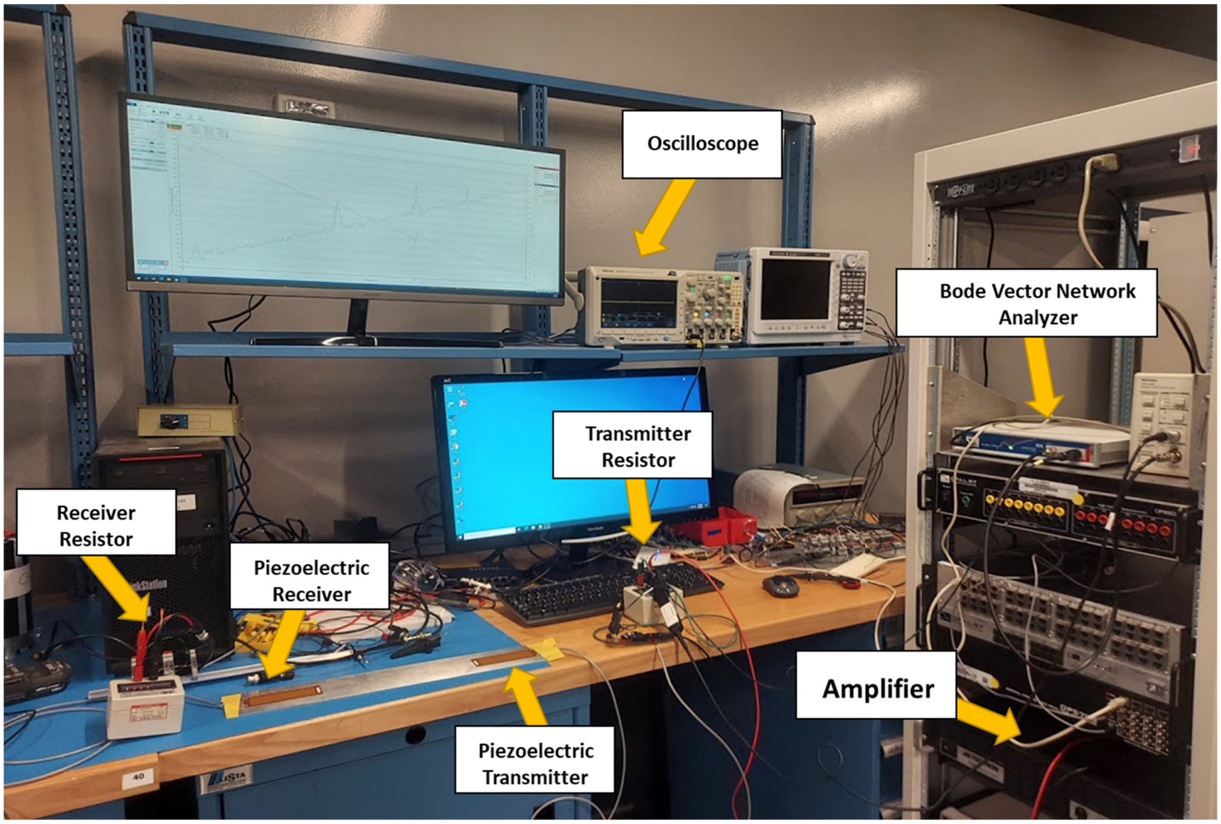

Figure 38: Updated Experimental Setup Using Bode Vector Network Analyzer

There is more room to do further experimental work and further refinement of the experimental setup that unfortunately was not completed due to delays caused by the limitations of lab access due to the quarantines put in place over the spring semester. Though the limitations of lab access resulted in delays in experimental analysis, the spring semester quarantine provided the opportunity to make progress in computational modeling of the complex power transfer system using a single transmitter and multiple receiver.

Complex Power Transfer System with Multiple Receiver Array

The second semester work of this project consisted of working to develop a complex power transfer system with selective pinging capabilities, by which a user can ping a specific, desired transducer. This complex system also focused on plate geometries as the medium for power transfer. Success in this endeavor added novelty to the project as extensive research had not been conducted on the ability to excite a specific transducer in a system with multiple transducers with a plate geometry. The approach for this final phase leveraged the computational parametric studies in terms of what parameters yield responsive and unresponsive systems. This intuition and understanding fed an attempt to design and analyze a system with multiple transducers with COMSOL using the intuition gained above. The success of the system is defined as the transfer of input vibrational energy to desired transducers and converted to electrical energy with appropriate efficiencies and power outputs.

Methodology of Complex Power Transfer System

The process of exploring the complex power transfer system leaned on lessons learned from the computational parametric studies. Figure 39 illustrates a model created to begin the complex power transfer system modeling process. This model was composed of a single transmitter and single receiver on a long plate that had overhang. The reasoning for this developed model was to analyze the strain field of the plate after conducting a frequency sweep over a range of interest.

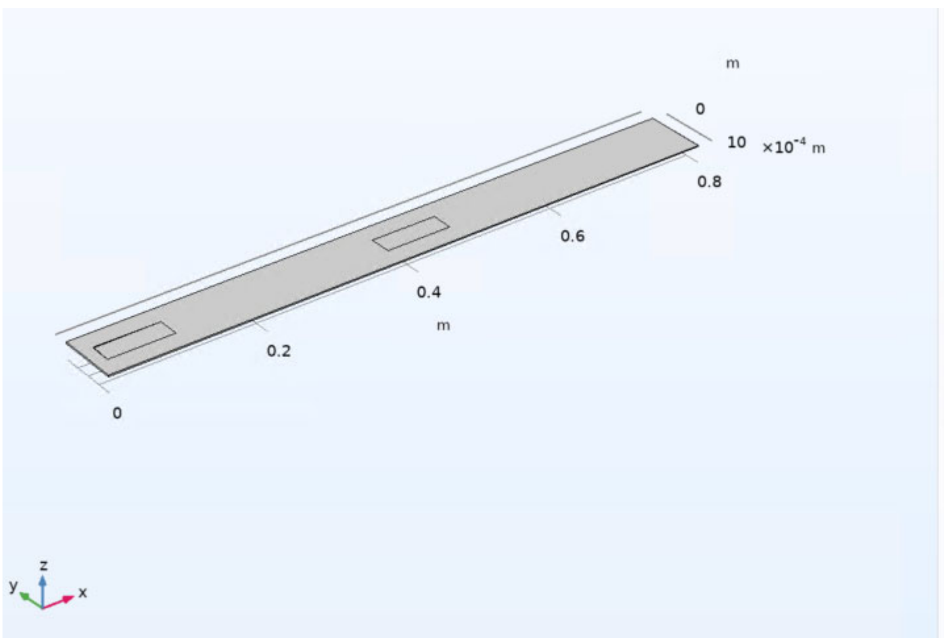

Figure 39: Schematic of Overhang Plate

Figure 40 illustrates the resulting strain field analysis from the frequency sweep for the plate with overhang.

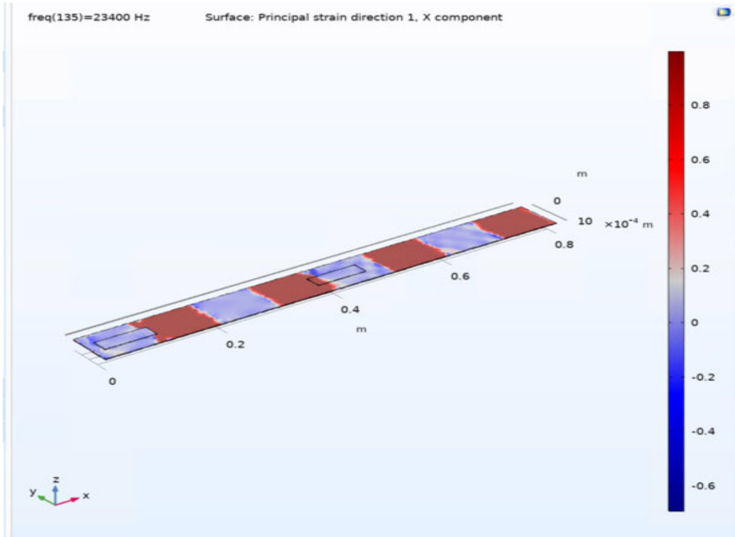

Figure 40: Strain Field Analysis for Plate with Overhang

This strain field analysis for the plate with overhang was an important first step in beginning the study of the complex transfer system. The strain field analysis allowed for the strains across the plate to be analyzed for unique frequencies. From this analysis, estimates on potential patch placement were made with the goal of placing the patches in locations where they would be uniquely excited. With these estimates, an initial complex COMSOL model was developed with a single transmitter and two receivers.

Figure 41 illustrates the complex system of interest with two piezoelectric receivers. The goal of the complex study is to use the piezoelectric transmitter to uniquely excite or ping a desired piezoelectric receiver without initiating a response from the undesired receiver.

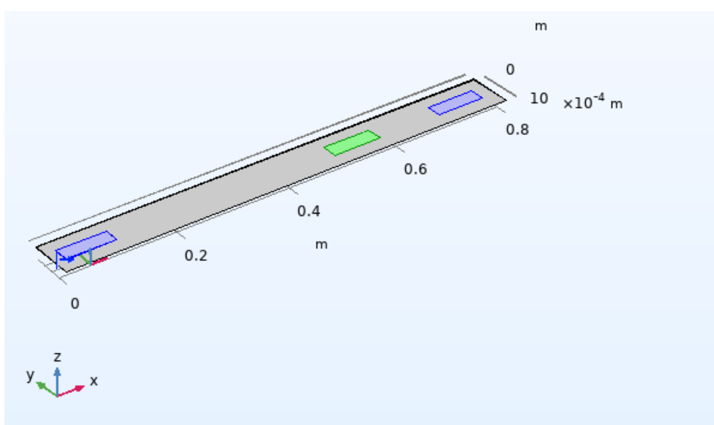

Figure 41: Initial COMSOL Model Used to Test Complex Power Transfer System with Two Piezoelectric Receivers

A frequency sweep was run with the system of two piezoelectric receivers using COMSOL Multiphysics. Figure 42 illustrates the initial sweep from 10kHz to 30kHz.

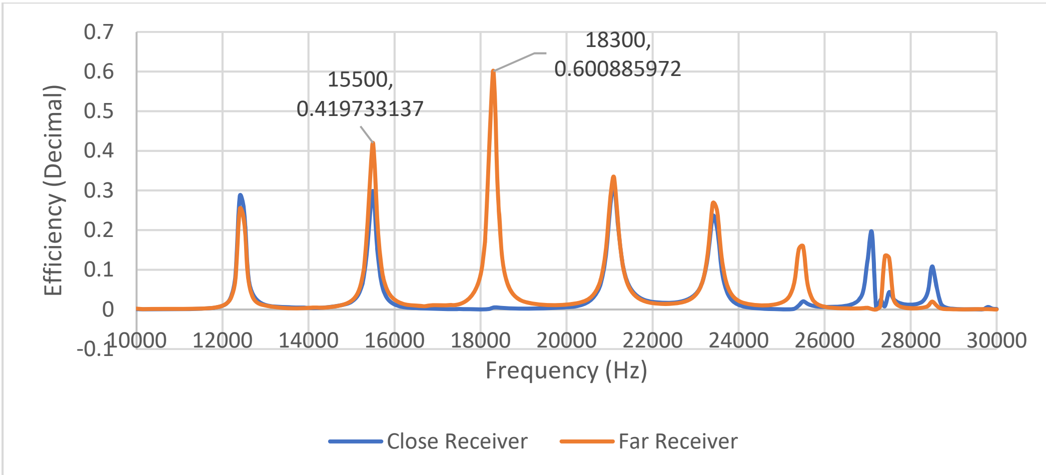

Figure 42: Efficiency vs Frequency of Initial Complex Power Transfer System with Two Receivers

In Figure 42, the close receiver is defined as the receiver closest to the piezoelectric transmitter and the far receiver is further from the transmitter. Figure 42 illustrates that at about 18.3 kHz the far receiver exhibits a point of peak with an efficiency of 60.1% where the close receiver exhibits a point of low efficiencies or a null. This would be a potential location that a user could selectively excite the close receiver while also avoiding a response from the far receiver. As illustrated by Figure 42, this initial configuration had an absence of a frequency to selectively excite the far receiver. Analysis of the strain fields at specific frequencies were used to determine an alternative configuration. Figure 43 illustrates an example plot of the strain field at 15.5 kHz to understand the spacing of the complex power transfer system. 15.5 kHz was specifically analyzed as it was a frequency in which both the close receiver and far receiver were simultaneously excited, which is undesired.

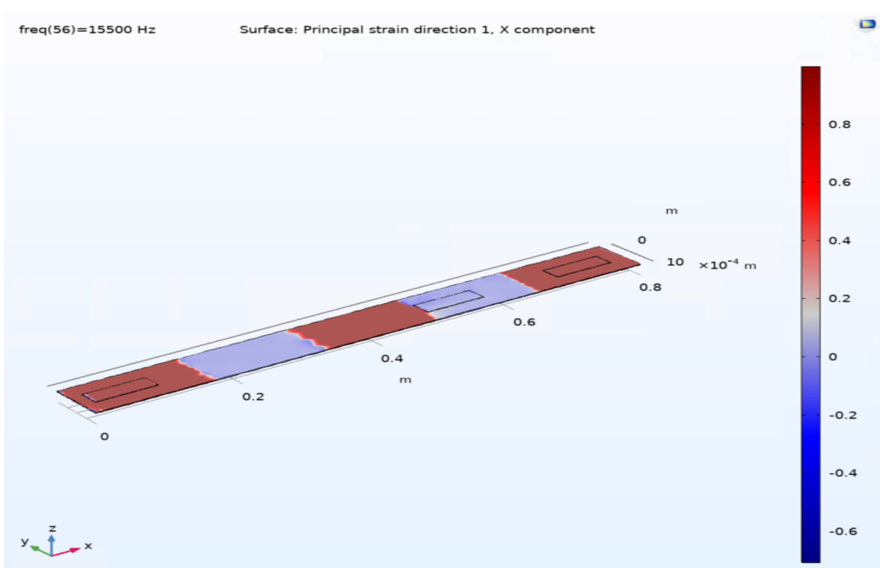

Figure 43: Plot of the Strain Field at 15.5 kHz for the Complex Power Transfer System

Figure 43 illustrates that both receivers are in a location where the net displacement is maximized as noted by both receivers being in a region of a solid color region. In the strain field plots, solid color regions corresponded to areas of maximum positive or negative strain. If both receivers are in a location of net maximum displacement they will both be excited, which is undesired. Figure 43 suggests that at least one of the patches needs to be shifted so the patch is not in a solid color region where there is maximum net displacement. Plots of the strain field for several frequencies were analyzed before determining a possible revised configuration with new spacing. The goal of the revised configuration was to place each receiver in a location where they would be uniquely excited at frequencies distinct from each other.

Figure 44 illustrates the changes in spacing that were determined based on the strain field analysis.

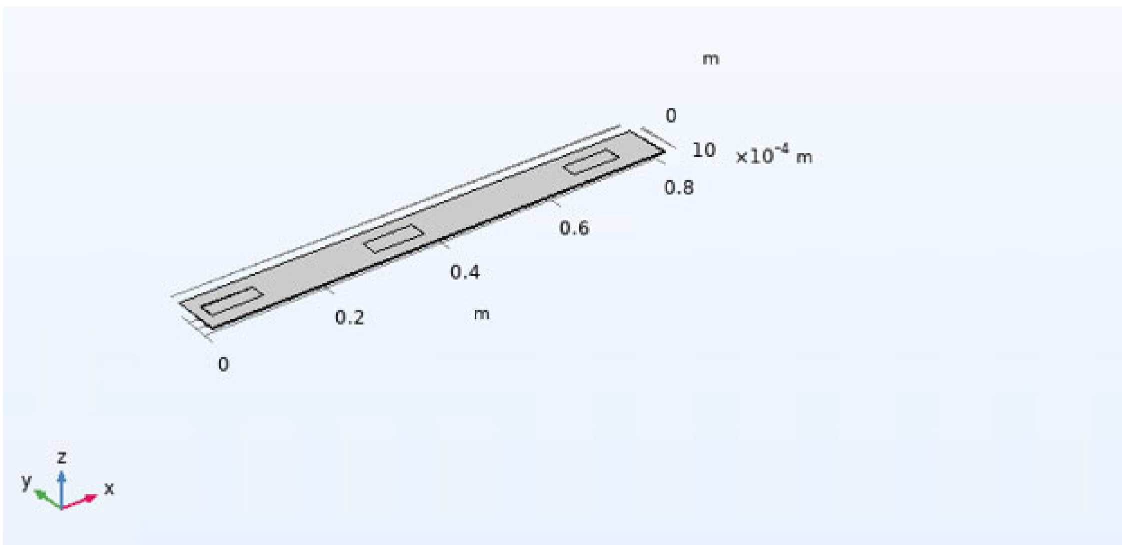

Figure 44: Updated Configuration for the Complex Power Transfer System with Two Receivers

After analyzing the strain fields, it was hypothesized that moving the two piezoelectric receivers to the left would better achieve the goal of selectively exciting a unique receiver. In comparison of Figure 41 and Figure 44, one can observe the differences in patch placement. Figure 45 illustrates the results of the frequency sweep for this updated patch placement.

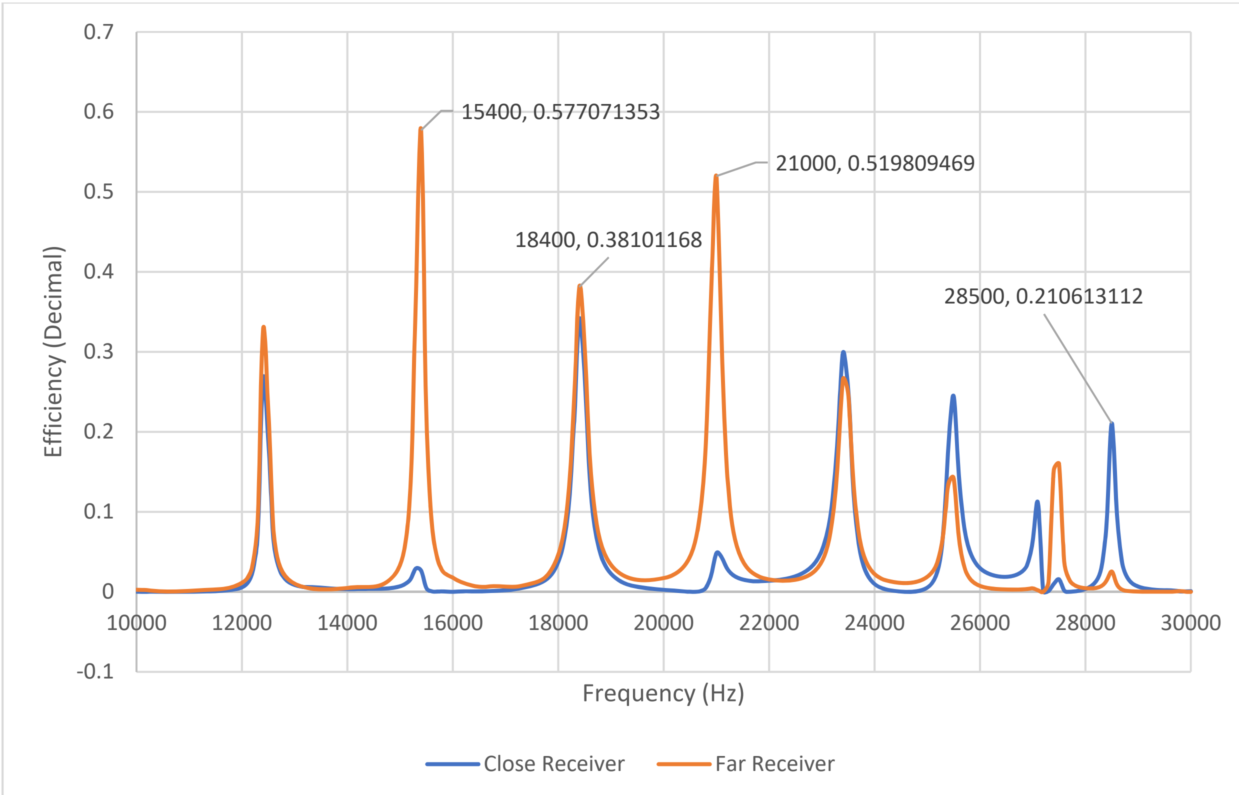

Figure 45: Results for Efficiency vs Frequency of Initial Complex Power Transfer System with Updated Patch Placement for the Two Receivers

Figure 45 illustrates two peaks of interest for the receiver at 15.4 kHz and 21 kHz that demonstrated high efficiencies without a significant response from the close receiver. At 28.5 kHz, the close receiver had a slight peak with an efficiency of 21% whereas the far receiver had a very small response at 28.5 kHz. This frequency provides an area of potential interest for selectively exciting the close receiver. Additionally, at 18.4 kHz, both the close and far receiver were excited with significant efficiencies. To optimize the system, a sweep of the efficiencies vs the load resistance was conducted for specific frequencies. Figure 46 illustrates an example of this sweep.

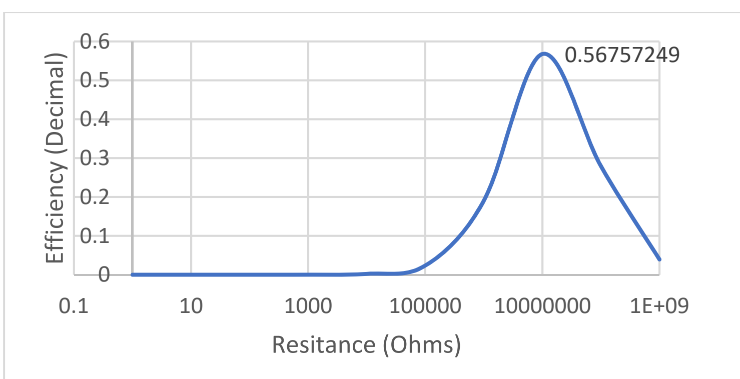

Figure 46: Initial Sweep of Efficiency vs Resistance for Far Receiver at 15.4 kHz

Figure 46 illustrates that a resistance value close to 10 megaohms optimizes the efficiency. After the initial sweeps for both the close and far receivers, finer sweeps were conducted and these optimized resistances were implemented to conduct another frequency sweep that is shown in Figure 47.

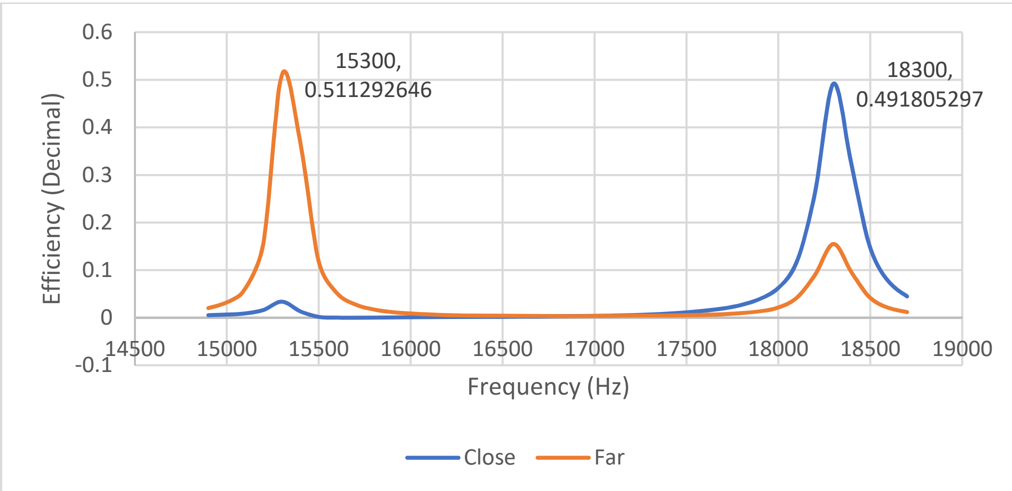

Figure 47: Efficiency vs Frequency for Complex Power Transfer System of Two Receivers After Optimizing the Resistances

Figure 47 illustrates that optimizing the resistance is an important step in achieving the ability to selectively excite a unique receiver. This final configuration that included optimized patch placement and resistors proved to be successful in achieving unique frequencies to selectively excite both the close and far receiver, at 18.3kHz and 15.3 kHz respectively.

Once success was demonstrated using two receivers, a more complex study was completed with three receivers. This was first tested by using piezoelectric receivers that had an active length of 56 mm rather than 85 mm. The smaller patches were initially used as it was expected that they would be easier to position in places where they would be uniquely excited.

Figure 48 illustrates the results of the initial frequency sweep from 10kHz to 30kHz for the complex power transfer system with three piezoelectric receivers with a length of 56 mm.

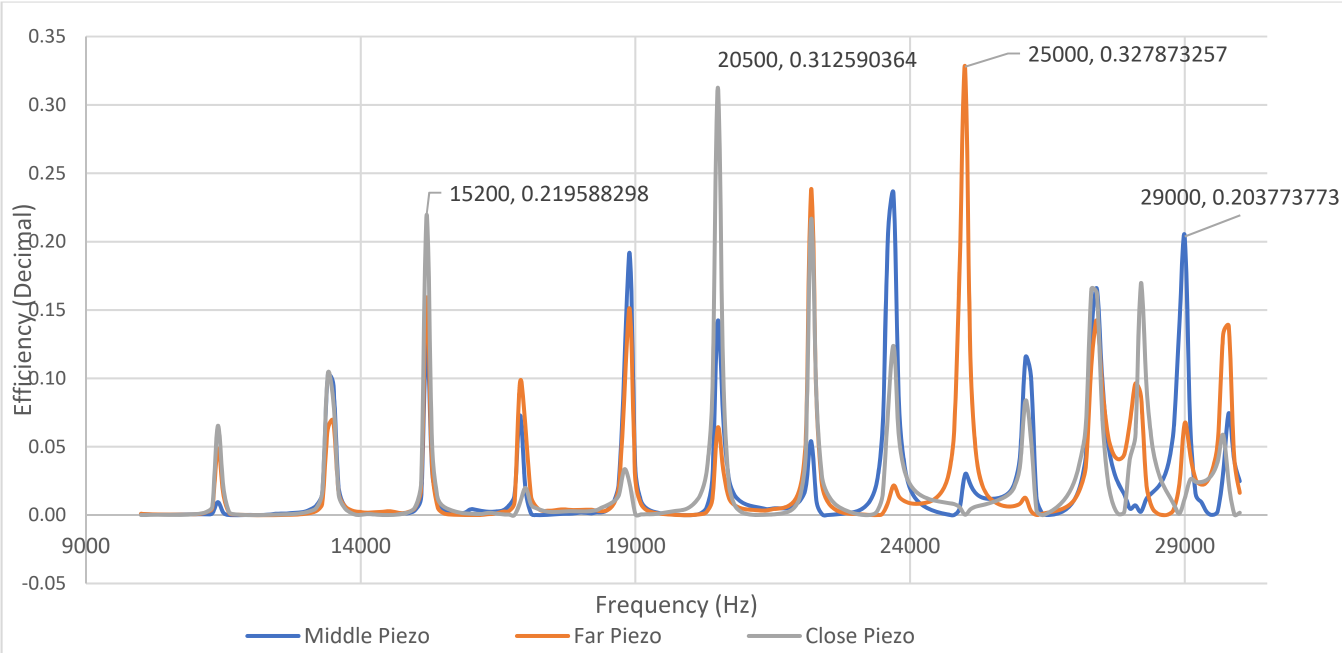

Figure 48: Plot of Efficiency vs Frequency for the Complex Power Transfer System with Three Piezoelectric Receivers with Length of 56 mm

Figure 48 illustrates several potential locations that could prove to be successful in uniquely exciting a specific receiver after further analysis and refinement of the configurations. After this initial sweep, the strain field plots for the potential frequencies of interest were studied and a revised configuration was determined. The model was updated with the modified patch placement and another frequency sweep was conducted. Figure 49 illustrates the results of the secondary sweep after updated patch placement.

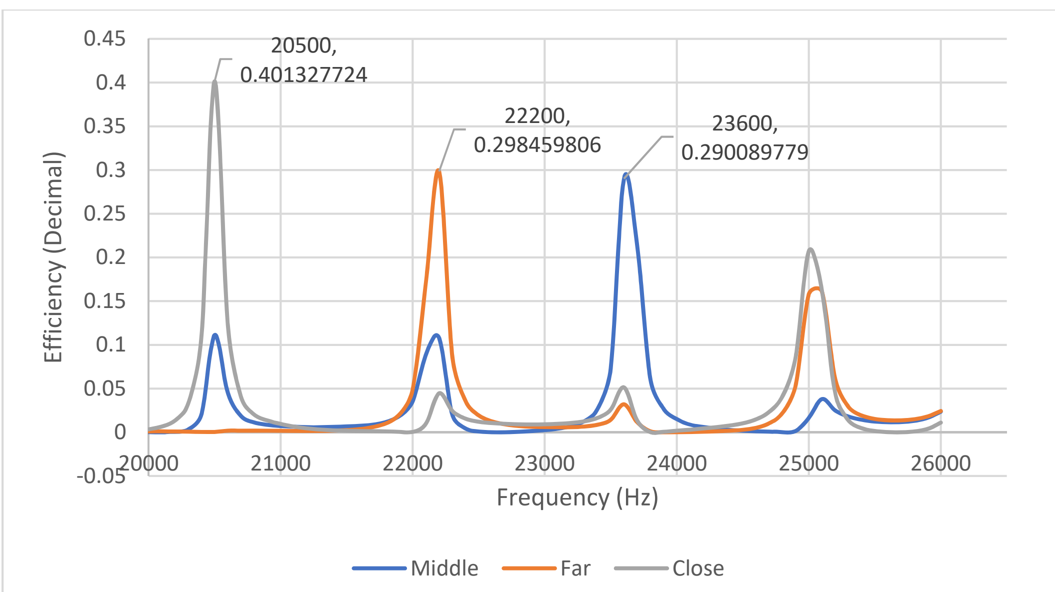

Figure 49: Secondary Sweep after Modified Patch Placement for the Complex Power Transfer System using Three Receivers with Patch Length of 56 mm

As Figure 49 illustrates, this modified patch placement produced promising unique frequencies that would allow selective excitation of the close, middle, and far receiver. After the study of the spacing proved to be successful, optimization studies for the resistance were conducted in a similar methodology as the studies conducted for the two receiver model. After optimized resistances were found, a new model was developed with the optimized patch placement and resistor values. The frequency sweep results are shown in Figure 50
.

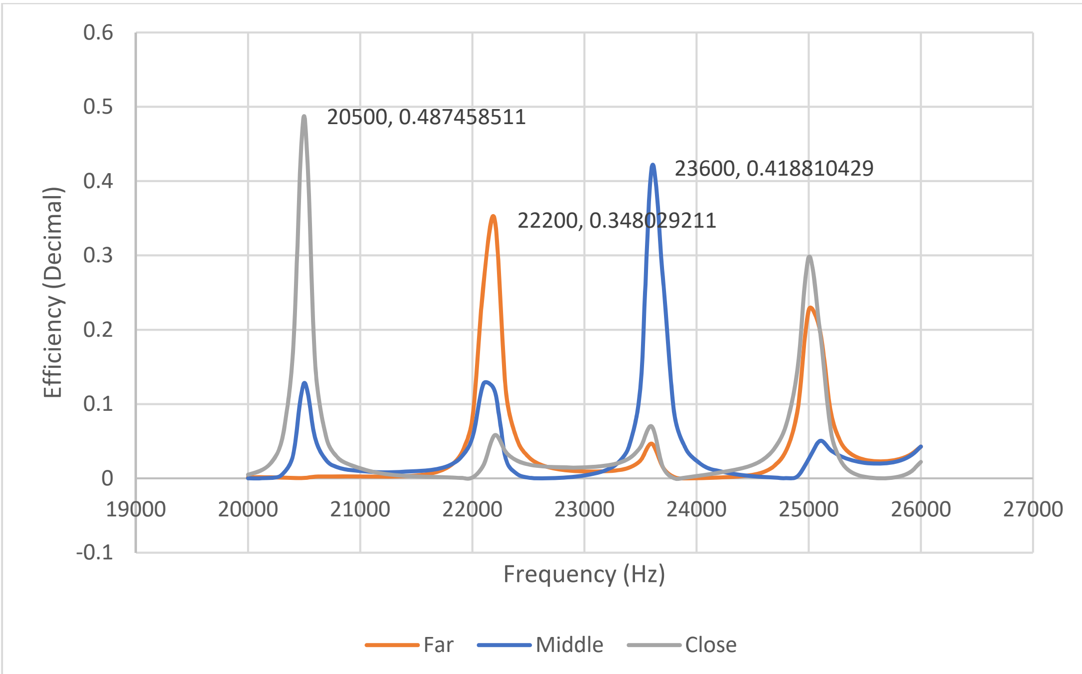

Figure 50: Efficiency vs Frequency for the Complex Power Transfer System using Three Receivers with Patch Length of 56 mm after Optimizing the Resistors and Patch Placement

As Figure 50 illustrates, the optimization of the resistors is a critical step in optimizing the efficiency of the response of the piezoelectric receivers and furthers the success of the complex power transfer system in the ability to uniquely excite a specific receiver.

A similar methodology was used in computationally studying a similar system that employed patches with length of 85 mm instead of 56mm. The lessons learned from modeling the system with 56mm were employed. The steps followed included an initial attempt on patch placement based on the 56mm studies. After a frequency sweep was conducted for this initial attempt, the strain field at specific frequencies was analyzed and the patch placement was modified in accordance with the strain field study. Another frequency sweep was conducted and the strain field study was analyzed with patch placement adjustments made as needed. This process was repeated several times until each receiver had unique peaks of excitation. After the positioning of the patches were finalized, the resistances for each receiver were optimized. The patches with 56mm were much easier to place in areas that they would be uniquely excited due to their smaller size as compared to the patches with length of 85mm.

Figure 51 illustrates the results of the initial model that was developed for patch length of 85mm.

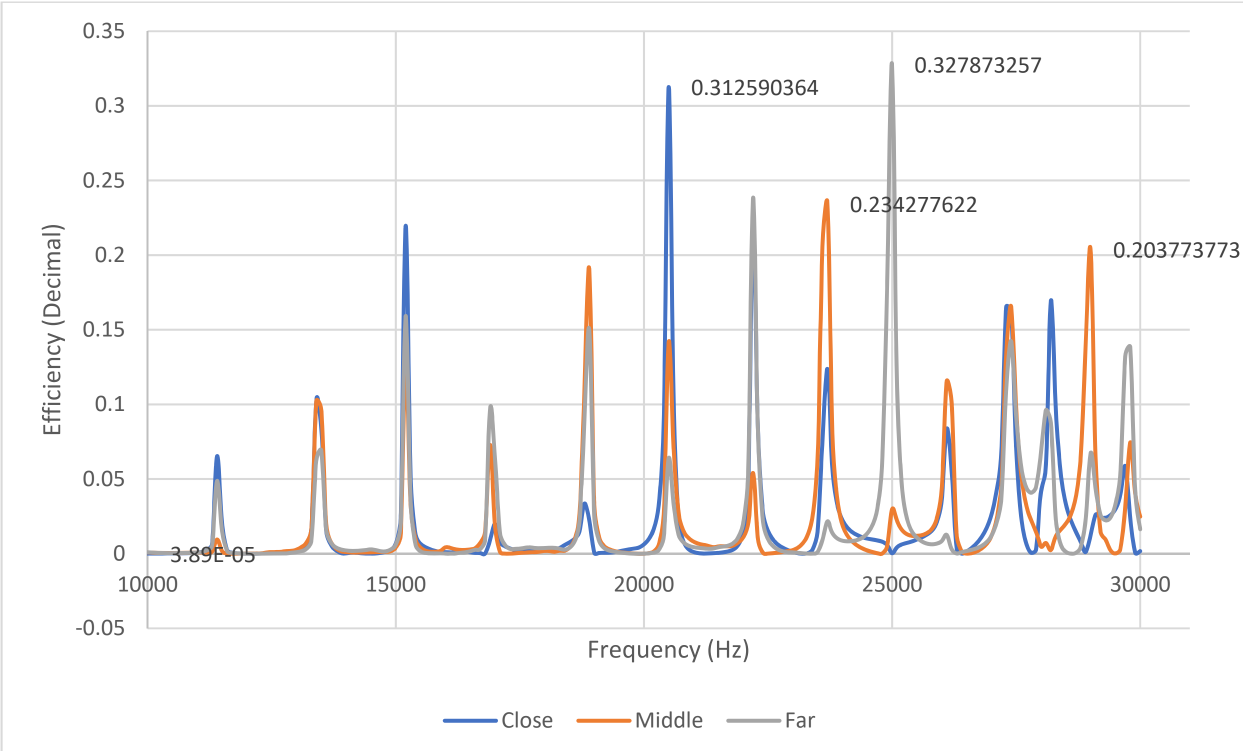

Figure 51: Results of Initial Complex Model for Patch Length of 85mm

Figure 52 illustrates the schematic of the complex power transfer system using three receivers and a single transmitter.

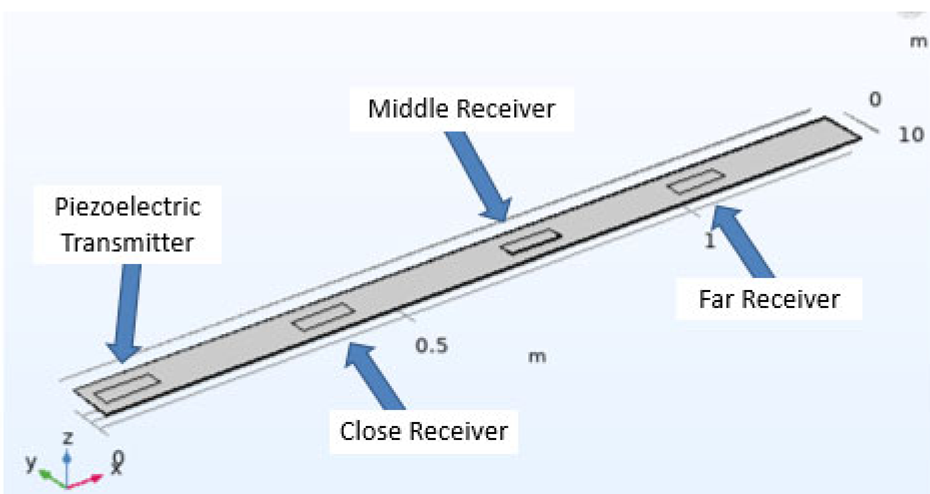

Figure 52: Schematic of Complex Power Transfer System Using a Single Transmitter and Three Receivers

Figure 53 illustrates the final results of the frequency sweep for the complex power transfer system using patches with length of 85mm. This final sweep represents the results after iterations of strain field analysis and revised patch placement and resistance optimization were conducted.

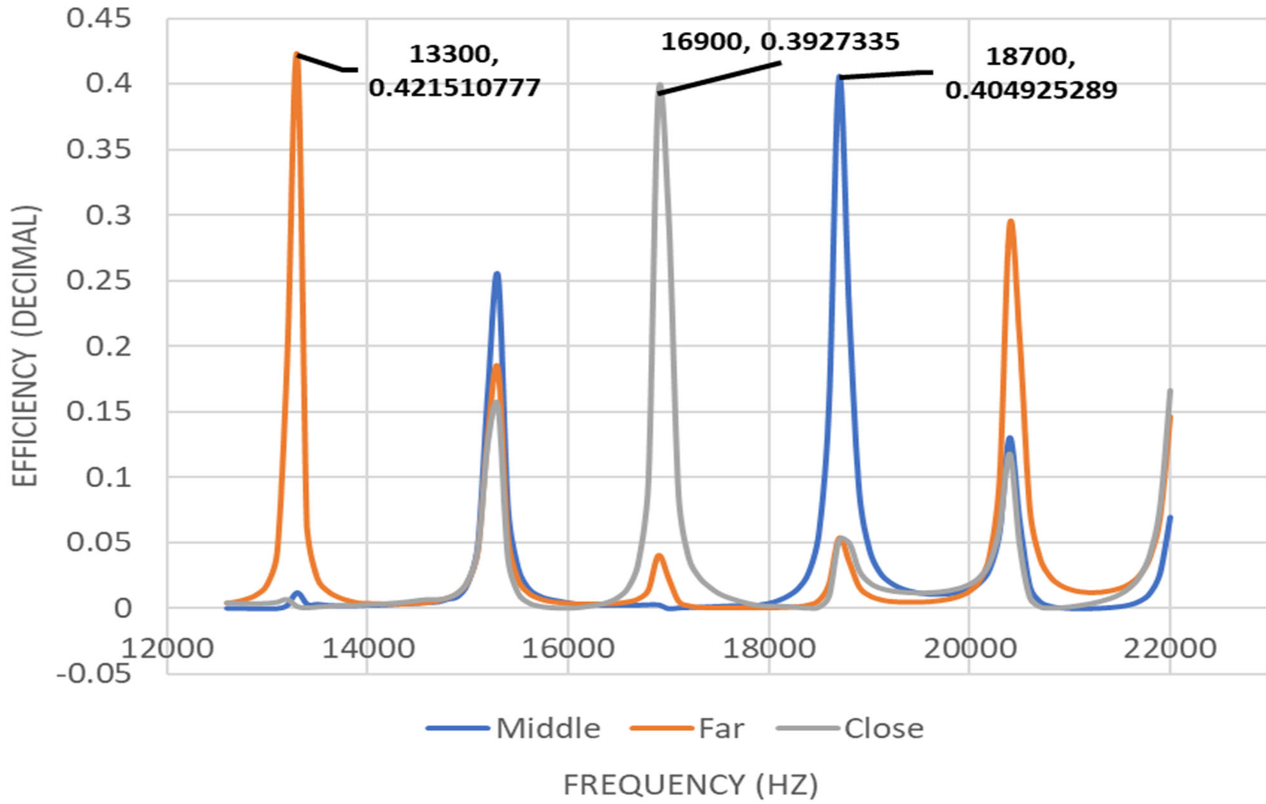

Figure 53: Final Frequency Sweep of Complex Power Transfer System Using a Single Transmitter and Three Receivers with Patch Length of 85mm

Future Work

Areas for future study include experimental analysis and validation of the computational results for the complex power transfer for both the 56mm and the 85mm case. Experimental validation and study would allow for further refinements to the complex and multiple receiver model. This analysis would also determine the effectiveness of the model in predicting the response for the complex power transfer system.

Additionally, experimental analysis of the symmetric power transfer system using axial waves by bonding a pair of piezoelectric patches on the bottom side of the plate offers another area of future study. It is expected that experimental results of the axial case would demonstrate broader peaks than the symmetric case.

Finally, a computational and experimental analysis of a complex power transfer system using axial waves for power transfer is an additional area of future study. To accomplish this a computational model would be developed first by placing a system of a single transmitter with multiple receivers on both the top and bottom of a parent structure, such as a plate. The computational study and analysis would offer the expected performance and could then be compared to and validated through experimental study of this complex case using axial waves for power transfer.

Conclusion

This project augments current research in piezoelectric materials and their application to power transfer systems. The computational model developed through COMSOL Multiphysics included considerations for solid mechanics, viscoelasticity, piezoelectricity, electrostatics, electrical circuits and by introducing structural acoustic coupling. Computational parametric studies were conducted that explored varying parameters such as the adhesive thickness, the adhesive material used, the material of the parent structure, symmetric vs axial wave transmission and the spacing between piezoelectric elements. Frequency sweeps were conducted for each of these studies and the electrical transfer efficiency, defined as the ratio of the power output to the power input, was studied. The parametric study of the adhesive thickness demonstrated that a thinner adhesive layer allows for larger peak efficiencies as thicker adhesive layer will absorb more of the mechanical energy than a thinner layer. From the parametric study on the material of the adhesive, it was determined that an adhesive material with a smaller tensile modulus will allow for higher efficiencies as the adhesives with larger tensile modulus tends to result in more undesired dissipation of the energy through the adhesive instead of the plate. The parametric study of the parent material demonstrated that variation in the parent material will result in variation of the magnitude and location of the peak efficiencies. Study of the symmetric vs asymmetric system demonstrated that a system that utilizes axial wave transmission through the symmetric system broadens the range of frequencies that a peak occurs at by suppressing flexural waves. Finally, the spacing computational studies demonstrated that the models with spacing between the piezoelectric patches greater than 0.277m tended to have peaks of greater magnitude. These lessons learned from these computational parametric studies proved to be of great utility in computationally modeling the single transmitter/multiple receiver system. Computational models were developed for patches of two different lengths that demonstrated the ability for a user to ping or selectively excite specific sensors, which allows for exciting applications to both the military and civilian sectors in systems that seek mass efficiency.

References

18-Minute Introduction to COMSOL Multiphysics®. (n.d.). COMSOL Multiphysics®. Retrieved February 4, 2020, from https://www.comsol.com/video/18-minute-introduction-to-comsol-multiphysics

1200px-Variable_resistor_symbol.svg.png (1200×960). (n.d.). [Web Image]. Retrieved February 25, 2020, from https://upload.wikimedia.org/wikipedia/commons/thumb/9/90/Variable_resistor_symbol.svg/1200px-Variable_resistor_symbol.svg.png

11005-05a.jpg (600×600). (n.d.). [Web Image]. Retrieved February 25, 2020, from https://cdn.sparkfun.com//assets/parts/6/2/6/2/11005-05a.jpg

Adhikari, S., Friswell, M. I., & Inman, D. J. (2009). Piezoelectric energy harvesting from broadband random vibrations. *Smart Materials and Structures*, *18*(11), 115005. https://doi.org/10.1088/0964-1726/18/11/115005

Allam, A., Sabra, K., & Erturk, A. (2019). Aspect ratio-dependent dynamics of piezoelectric transducers in wireless acoustic power transfer. *IEEE Transactions on Ultrasonics, Ferroelectrics, and Frequency Control*, *Journal Article*, 1–1. https://doi.org/10.1109/TUFFC.2019.2962711

Aryan, P., Kotousov, A., Ng, C.T., & Cazzolato, B.S. (2019). Lamb wave characterisation and damage imaging for isotropic plate-like structures using 3D laser vibrometry. Recent Advances in Structural Integrity Analysis - Proceedings of the International Congress (APCF/SIF-2014),Woodhead Publishing. https://www.sciencedirect.com/science/article/pii/B9780081002032501169

Beyond Biohazard: Why Danger Symbols Can't Last Forever—99% Invisible. (n.d.). [Web Image]. Retrieved February 25, 2020, from https://99percentinvisible.org/article/beyond-biohazard-danger-symbols-cant-last-forever/

Čeponis, A., Mažeika, D., & Kilikevičius, A. (2019). Bidirectional Piezoelectric Energy Harvester. *Sensors (Basel, Switzerland)*, *19*(18), 3845. https://doi.org/10.3390/s19183845

Chang, Z., Bao, X., Doty, B. J., Sherrit, S., Bar-Cohen, Y., Badescu, M., & Aldrich, J. (2007). Power loss consideration in wireless piezoelectric acoustic-electric power feedthru. *Proceedings of SPIE*, *6529*, 652942–652946. https://doi.org/10.1117/12.716433

Chen, S.-M., Zhou, J.-J., & Hu, J.-H. (2014). Experimental study and finite element analysis for piezoelectric impact energy harvesting using a bent metal beam. *International Journal of Applied Electromagnetics and Mechanics*, *46*(4), 895–904. https://doi.org/10.3233/JAE-140097

Components, E. and E. (n.d.). *Energy Harvesting | Würth Elektronik: Electronic & Electromechanical Components > Products & Services > Applications > Energy Harvesting > Gleanergy* [Web Image]. Retrieved February 25, 2020, from https://www.we-online.com/web/en/electronic_components/produkte_pb/demoboards/energy_harvesting/gleanergy/gleanergy.php

Cottone, F., Gammaitoni, L., Vocca, H., Ferrari, M., & Ferrari, V. (2012). Piezoelectric buckled beams for random vibration energy harvesting. *Smart Materials and Structures*, *21*(3), 35021. https://doi.org/10.1088/0964-1726/21/3/035021

Dagdeviren, C., Yang, B. D., Su, Y., Tran, P. L., Joe, P., Anderson, E., Xia, J., Doraiswamy, V., Dehdashti, B., Feng, X., Lu, B., Poston, R., Khalpey, Z., Ghaffari, R., Huang, Y., Slepian, M. J., & Rogers, J. A. (2014). Conformal piezoelectric energy harvesting and storage from motions of the heart, lung, and diaphragm. *Proceedings of the National Academy of Sciences of the United States of America*, *111*(5), 1927–1932. https://doi.org/10.1073/pnas.1317233111

Elfrink, R., Kamel, T. M., Goedbloed, M., Matova, S., Hohlfeld, D., van Andel, Y., & van Schaijk, R. (2009). Vibration energy harvesting with aluminum nitride-based piezoelectric devices. *Journal of Micromechanics and Microengineering*, *19*(9), 094005. https://doi.org/10.1088/0960-1317/19/9/094005

Freiman, S. W., & White, G. S. (1995). Intelligent Ceramic Materials: Issues of Brittle Fracture. *Journal of Intelligent Material Systems and Structures*, *6*(1), 49–54.

Friswell, M. I., & Adhikari, S. (2010). Sensor shape design for piezoelectric cantilever beams to harvest vibration energy. *Journal of Applied Physics*, *108*(1), 014901-014901–014906. https://doi.org/10.1063/1.3457330

Gas Lighter Gun For Gas-stove On A White Background Stock Photo, Picture And Royalty Free

Image. Image 58977063. (n.d.). [Web Image]. Retrieved February 25, 2020, from https://www.123rf.com/photo_58977063_gas-lighter-gun-for-gas-stove-on-a-white-background.html

Giannelli, P., Bulletti, A., & Capineri, L. (2016). Charge-mode interfacing of piezoelectric interdigital Lamb wave transducers. *Electronics Letters*, *52*(11), 894–896. https://doi.org/10.1049/el.2016.0804

Hajati, A., & Kim, S.-G. (2011). Ultra-wide bandwidth piezoelectric energy harvesting. *Applied Physics Letters*, *99*(8), 083105-083105–3. https://doi.org/10.1063/1.3629551

Hameed, M. S., Li, Z., Chen, J., & Qi, J. (2019). Lamb-Wave-Based Multistage Damage Detection Method Using an Active PZT Sensor Network for Large Structures. *Sensors (Basel, Switzerland)*, *19*(9), 2010. https://doi.org/10.3390/s19092010

Helmand_troops_web_large-1860x930.jpg (1860×930). (n.d.). [Web Image]. Retrieved February 25, 2020, from https://ceobs.org/wp-content/uploads/2019/10/helmand_troops_web_large-1860x930.jpg

Hong, Y. K., & Moon, K. S. (2005). Single crystal piezoelectric transducers to harvest vibration energy. *Proceedings of SPIE*, *6048*, 60480E-60480E – 7. https://doi.org/10.1117/12.650612

Howells, C. A. (2009). Piezoelectric energy harvesting. *Energy Conversion and Management*, *50*(7), 1847–1850. https://doi.org/10.1016/j.enconman.2009.02.020

Jalili, N. (2010). *Piezoelectric-based vibration-control: From macro to micro/nano scale systems*. Springer. http://usna.summon.serialssolutions.com/2.0.0/link/0/eLvHCXMwdV2xbgIxDLUQLHRqKYiWUrF0PJS7ixM8owJTBQKxouPiSCwwoHZg4NtJcne0qmCMIlmOFeXFL_EzQJoMRfTvTBgx50JqtsY6wKTMkkuHMne11UIaDhTvYoFfY1xN1bSU3T7-UhnD7-M-u36rCdSF0hJjfV56KVAk9HnXaE1XekWkOsEEQymXdKAnFMWVwlM5LqT3qr44AU8mj1D3NQZPUON9Cx7-aAI-w8d8x6dD0Z1ml0ceZczgxzvoQxiVX8vb0J98rsazyJvelBzMpvJXJR2ou7yeuzCQ-ZY0olHxlqRBJhcMladoTUaGNb1A57aN13sTPWgWj9ueIXiDhnU7mPvFKt9DfC6SKmxr

Juan, W., Hongsheng, H., Suxiang, Q., & Linfang, Q. (2007). Research on Shape Control and Active Vibration Control of Piezoelectric Composite Laminated Shell. *2007 8th International Conference on Electronic Measurement and Instruments*, 4–569. https://doi.org/10.1109/ICEMI.2007.4351208

Jung, J. H., Lee, M., Hong, J.-I., Ding, Y., Chen, C.-Y., Chou, L.-J., & Wang, Z. L. (2011). Lead-Free NaNbO3 Nanowires for a High Output Piezoelectric Nanogenerator. *ACS Nano*, *5*(12), 10041–10046. https://doi.org/10.1021/nn2039033

Kural, A., Pullin, R., Holford, K., Lees, J., Naylon, J., Paget, C., & Featherston, C. (2013). Design and characterization of an ultrasonic lamb-wave power delivery system. *IEEE Transactions on Ultrasonics, Ferroelectrics, and Frequency Control*, *60*(6), 1134–1140. https://doi.org/10.1109/TUFFC.2013.2676

Lawry, T. J., Wilt, K. R., Ashdown, J. D., Scarton, H. A., & Saulnier, G. J. (2013). A high-performance ultrasonic system for the simultaneous transmission of data and power through solid metal barriers. *IEEE Transactions on Ultrasonics, Ferroelectrics, and Frequency Control*, *60*(1), 194–203. https://doi.org/10.1109/TUFFC.2013.2550

Lee, B. Y., Zhang, J., Zueger, C., Chung, W.-J., Yoo, S. Y., Wang, E., Meyer, J., Ramesh, R., & Lee, S.-W. (2012). Virus-based piezoelectric energy generation. *Nature Nanotechnology*, *7*(6), 351–356. https://doi.org/10.1038/nnano.2012.69

Lin, J.-C., & Nien, M. H. (2005). Adaptive control of a composite cantilever beam with piezoelectric damping-modal actuators/sensors. *Composite Structures*, *70*(2), 170–176. https://doi.org/10.1016/j.compstruct.2004.08.020

Lin, S., Cao, H., & Qiao, X. (2016). Wireless Power Transmission Based on Sandwiched Composite Piezoelectric Transducers in Length Extensional Vibration. *IEEE Transactions on Power Electronics*, *31*(9), 6134–6143. https://doi.org/10.1109/TPEL.2015.2502586

Liu, G. R., Peng, X. Q., Lam, K. Y., & Tani, J. (1999). VIBRATION CONTROL SIMULATION OF LAMINATED COMPOSITE PLATES WITH INTEGRATED PIEZOELECTRICS. *Journal of Sound and Vibration*, *220*(5), 827–846. https://doi.org/10.1006/jsvi.1998.1970

Mahbub, I., Pullano, S. A., Wang, H., Islam, S. K., Fiorillo, A. S., To, G., & Mahfouz, M. R. (2017). A Low-Power Wireless Piezoelectric Sensor-Based Respiration Monitoring System Realized in CMOS Process. *IEEE Sensors Journal*, *17*(6), 1858–1864. https://doi.org/10.1109/JSEN.2017.2651073

Mehraeen, S., Jagannathan, S., & Corzine, K. A. (2010). Energy Harvesting From Vibration With Alternate Scavenging Circuitry and Tapered Cantilever Beam. *IEEE Transactions on Industrial Electronics*, *57*(3), 820–830. https://doi.org/10.1109/TIE.2009.2037652

Monaco, E., Memmolo, V., Ricci, F., Boffa, N. D., & Maio, L. (2015). *Guided waves based SHM systems for composites structural elements: Statistical analyses finalized at probability of detection definition and assessment*. *9438*, 94380M-94380M – 11. https://doi.org/10.1117/12.2084334

NASA-Tv.jpg (756×554). (n.d.). [Web Image]. Retrieved February 25, 2020, from https://www.panoramaaudiovisual.com/wp-content/uploads/2016/02/NASA-Tv.jpg

Qi, Y., Jafferis, N. T., Lyons, K., Lee, C. M., Ahmad, H., & McAlpine, M. C. (2010). Piezoelectric Ribbons Printed onto Rubber for Flexible Energy Conversion. *Nano Letters*, *10*(2), 524–528. https://doi.org/10.1021/nl903377u

QIU, L., YAN, X., LIN, X., & YUAN, S. (2019). Multiphysics simulation method of lamb wave propagation with piezoelectric transducers under load condition. *Chinese Journal of Aeronautics*, *32*(5), 1071–1086. https://doi.org/10.1016/j.cja.2019.02.007

Radice, Joshua J., Tseng, V., Drummond, T., Diamond, D., Schieuer, N., Bedair, Sarah. (11/2020). "Multiphysics modeling of ultrasonic elastic wave attenuation for wireless power transfer including viscoelasticity and acoustic emission". Mechanics Research Communications (0093-6413), p. 103600.

Rahman, L. (2017). *Is this the future for medical implants?* [Web Image]. https://www.med-technews.com/api/content/7bf93d8a-370c-11e7-a67a-0aea2a882f79/

Ramadan, K. S., Sameoto, D., & Evoy, S. (2014). A review of piezoelectric polymers as functional materials for electromechanical transducers. *Smart Materials and Structures*, *23*(3), 33001. https://doi.org/10.1088/0964-1726/23/3/033001

Randeraat, J. van. (1968). *Piezoelectric ceramics*. Mullard Limited. http://usna.summon.serialssolutions.com/2.0.0/link/0/eLvHCXMwY2AwNtIz0EUrEywsDY2MLIGVsWGaRUqSoWWypYVZimmKMegiPmAdD-o3Bgaa-jmbhribuUOP3S5GDGXolRbnJcKX1YCHLkDz9uaGdcGgo0BNLU1B_S6LMEvwaXqwq27AVYSbIAMLaNuAEANTap4Ig1hAZmpVPuSKmcxkheTUItC178WiDLJuriHOHrog3fHQkZN4mC0GRmIMLMDeeKoEg4IRaNmuhbEZ6MYWE_PExEQjw0RLM0vTx

EQLS4uktBRJBjHsZkjhkpBm4AJmAwtIv16GgTUNmO5SZSEekQP7CgAYllfc

Saadon, S., & Sidek, O. (2011). A review of vibration-based MEMS piezoelectric energy harvesters. *Energy Conversion and Management*, *52*(1), 500–504. https://doi.org/10.1016/j.enconman.2010.07.024

Sankman, J., & Ma, D. (2015). A 12-?W to 1.1-mW AIM piezoelectric energy harvester for time-varying vibrations with 450-nA I_{bm Q}. *IEEE Transactions on Power Electronics*, *30*(2), 632.

Science, 4Test Measurement. (n.d.). *Keysight E4990A Impedance Analyzer—4Test AS* [Web Image]. Retrieved February 25, 2020, from https://www.4test.no/Keysight+E4990A+Impedance+Analyzer.htm

Scope-probes-500x500.jpg (500×500). (n.d.). [Web Image]. Retrieved February 25, 2020, from https://www.hobbytronics.co.uk/image/cache/data/ht/scope-probes-500x500.jpg

Sdg6000x-1000x1000.png (1000×1000). (n.d.). [Web Image]. Retrieved February 25, 2020, from https://www.batterfly.com/shop/image/cache/catalog/pic%20siglent/sdg/sdg6000x/sdg6000x-1000x1000.png

Sensors-09-04195f1.png (1000×642). (n.d.). [Web Image]. Retrieved February 25, 2020, from https://www.mdpi.com/sensors/sensors-09-04195/article_deploy/html/images/sensors-09-04195f1.png

Shahab, S., & Erturk, A. (2014). Contactless ultrasonic energy transfer for wireless systems: Acoustic-piezoelectric structure interaction modeling and performance enhancement. *Smart Materials and Structures*, *23*(12), 125032. https://doi.org/10.1088/0964-1726/23/12/125032

Sideridis, E., Prassianakis, I. N., & Kytopoulos, V. N. (2006). Storage and loss moduli behavior of plasticized epoxy polymers over a frequency and temperature range, and damaging effects assessment by means of the NDT method of ultrasounds and moisture absorption. *Journal of Applied Polymer Science*, *101*(6), 3869–3880. https://doi.org/10.1002/app.24525

Smart structures. (n.d.). [Web Image]. Retrieved February 25, 2020, from https://wsnblog.wordpress.com/tag/smart-structures/

Stobbe, D.M., Grünsteidl, C.M. & Murray, T.W. Propagation and Scattering of Lamb Waves at Conical Points in Plates. Sci Rep 9, 15216 (2019). https://doi.org/10.1038/s41598-019-51187-9

Su Z., Ye L. (2009) Fundamentals and Analysis of Lamb Waves. In: Identification of Damage Using Lamb Waves. Lecture Notes in Applied and Computational Mechanics, vol 48. Springer, London. https://doi.org/10.1007/978-1-84882-784-4_2

Tseng, V. F.-G., Bedair, S. S., Radice, J., Drummond, T. E., & Lazarus, N. (2019). Ultrasonic Lamb Waves for Wireless Power Transfer. *IEEE XPlore Digital Library*. www.ieeexplore.ieee.org/document/8882371

Vijaya, M. S. (2013). *Piezoelectric materials and devices: Applications in engineering and medical sciences*. CRC Press. http://usna.summon.serialssolutions.com/2.0.0/link/0/eLvHCXMwdV09iwIxEB1Em7Py48TPY8Fa2SRkk9SLetVxcnKtJG4CNlosNhb-difZXRXRMgTCJMxk5j2SNwCMzuPZ053ApNOMOOUIyYgwMTGUCZE4yY3WMvNMwXrNf1K-WSWrUnY7v1MZ81N-0LdnNZ66oJjnhKKXPy8FyhX3uEv-qxu9gp7MMXmGr1xMYSTJhFQKT-VYBum9qi9OyCfLFtT9H4M21OyhA80HTcAuTH_39nwsutPsdxEWlIWPRAj5o8yGwP

6EyXKxSb9nfuFtycBsK2sp7UEdUb3tQ6SxlHCx3SnqMY0zOlEcgS03AjOmE2wAvddrDN9NjOCDhl4Nnh8YQ8OhbXZS7PErnM4VQo1rEA

Wang, X., Shi, Z., & Song, G. (2019). Analytical study of influence of boundary conditions on acoustic power transfer through an elastic barrier. *Smart Materials and Structures*, *28*(2), 25004. https://doi.org/10.1088/1361-665X/aaeb73

Wang, Y., Wang, L., Cheng, T., Song, Z., & Qin, F. (2016). Sealed piezoelectric energy harvester driven by hyperbaric air load. *Applied Physics Letters*, *108*(3), 33902. https://doi.org/10.1063/1.4940199

Wang, Z. L., Dai, L., Yang, R., & Qin, Y. (2009). Power generation with laterally packaged piezoelectric fine wires. *Nature Nanotechnology*, *4*(1), 34–39. https://doi.org/10.1038/nnano.2008.314

Zhou, S., Cao, J., Erturk, A., & Lin, J. (2013). Enhanced broadband piezoelectric energy harvesting using rotatable magnets. *Applied Physics Letters*, *102*(17), 173901. https://doi.org/10.1063/1.4803445

Image References:

(*1200px-Variable_resistor_symbol.svg.png (1200×960)*, n.d.)
(*11005-05a.jpg (600×600)*, n.d.)
(*Beyond Biohazard: Why Danger Symbols Can’t Last Forever—99% Invisible*, n.d.)
(Components, n.d.)
(Components, n.d.)
(*Gas Lighter Gun For Gas-stove On A White Background Stock Photo, Picture And Royalty Free Image. Image 58977063.*, n.d.)
(*Helmand_troops_web_large-1860x930.jpg (1860×930)*, n.d.)
(*NASA-Tv.jpg (756×554)*, n.d.)
(Rahman, 2017)
(Science, n.d.)
(*Scope-probes-500x500.jpg (500×500)*, n.d.)
(*Sdg6000x-1000x1000.png (1000×1000)*, n.d.)
(*Sensors-09-04195f1.png (1000×642)*, n.d.)
(*Smart structures*, n.d.)